Chen *et al. Microstructures* **2025**, *5*, 2025084
DOI: 10.20517/microstructures.2025.10

Microstructures

Review

Open Access

Check for updates

Recent advances of conversion-type iron-based materials for sodium-ion batteries

Suping Chen[1], Shiying Ye[1], Xijun Xu[1], Weizhen Fan[2], Jingwei Zhao[2], Huapeng Sun[3], Yanping Huo[1,4]

[1]School of Chemical Engineering and Light Industry, Guangdong University of Technology, Guangzhou 510006, Guangdong, China.
[2]Research and Development Center, Guangzhou Tinci Materials Technology Co., Ltd., Guangzhou 510765, Guangdong, China.
[3]School of New Energy, Chenzhou Vocational Technical College, Chenjiang Laboratory, Chenzhou 423000, Hunan, China.
[4]Analytical & Testing Center, Guangdong University of Technology, Guangzhou 510006, Guangdong, China.

Correspondence to: Dr. Xijun Xu, School of Chemical Engineering and Light Industry, Guangdong University of Technology, 100 Waihuan Xi Road, Panyu District, Guangzhou 510006, Guangdong, China. E-mail: xuxijun2022@gdut.edu.cn; Prof./Dr.Yanping Huo, School of Chemical Engineering and Light Industry, Guangdong University of Technology, 100 Waihuan Xi Road, Panyu District, Guangzhou 510006, Guangdong, China. E-mail: yphuo@gdut.edu.cn; Dr. Huapeng Sun, School of New Energy, Chenzhou Vocational Technical College, Chenjiang Laboratory, No. 909, Chenzhou Avenue, Wangxianling, Chenzhou 423000, Hunan, China. E-mail: huapengsun@hotmail.com

How to cite this article: Chen, S.; Ye, S.; Xu, X.; Fan, W.; Zhao, J.; Sun, H.; Huo, Y. Recent advances in conversion-type iron-based materials for sodium-ion batteries. *Microstructures* **2025**, *5*, 2025084. https://dx.doi.org/10.20517/microstructures.2025.10

Received: 7 Feb 2025 **First Decision:** 9 Apr 2025 **Revised:** 22 Apr 2025 **Accepted:** 9 May 2025 **Published:** 18 Jul 2025

Academic Editor: Zaiping Guo **Copy Editor:** Fangling Lan **Production Editor:** Fangling Lan

Abstract

Lithium-ion batteries have come to dominate the secondary energy storage market; however, their broader application is limited by the scarcity of lithium resources and high production costs. As a promising alternative, sodium-ion batteries (SIBs) have attracted significant attention due to their similar electrochemical behavior and the abundant availability of sodium-based raw materials. It is well recognized that the electrode material plays a crucial role as it directly influences the overall cycle life of the battery. Iron-based materials are particularly attractive due to their abundant raw material availability, cost-effectiveness, safety profile, and environmental friendliness; thus, they represent one of the most suitable classes of electrode materials. Recently, many studies have focused on designing appropriate nanostructures and developing straightforward methods for improving the electrochemical features of conversion-type iron-based electrodes. This review summarizes recent advancements in iron-based electrodes for SIBs and outlines future directions for the advancement of conversion-type iron-based materials. It is expected to provide valuable insights for the design of high-performance iron-based electrodes for SIBs.

Keywords: Iron-based electrodes, sodium-ion batteries, nanostructures, carbon coating, metal-organic frameworks

INTRODUCTION

The growing popularity of low-carbon and environmentally friendly lifestyles has led to increasing demand for highly efficient energy storage devices. Currently, lithium-ion batteries (LIBs) are widely utilized in mobile phones, laptops, and other portable electronic devices due to their long service life, high operating voltage, and high energy density[1-3]. With the continuous enhancement of cycle performance and safety features, LIBs have demonstrated significant potential across various fields, including aerospace, electromobility, and large-scale electrochemical energy storage systems[1-3]. As a result, improving the electrochemical properties of rechargeable batteries remains a central focus of current research. In practical applications, consumers primarily seek cost-effective batteries with long service lives. However, it is noteworthy that most lithium salts required for LIB production are concentrated in plateau regions, where mining poses considerable challenges[4,5]. This reality makes it essential to identify alternative battery systems that offer abundant raw material availability, low cost, and favorable electrochemical properties. Among such candidates, sodium-ion batteries (SIBs) have emerged as a compelling option owing to the abundance of sodium resources, their lower cost, and electrochemical behavior similar to LIBs[6,7]. Research interest in SIBs has grown significantly in recent years. To optimize sodium utilization and further reduce battery costs, it is particularly crucial to identify low-cost electrode materials derived from abundant raw sources and enhance their electrochemical performance[8-10].

Iron is the second most abundant metal in the Earth's crust, second only to aluminum. Compared to currently commercialized anode and cathode materials, iron-based electrodes offer several advantages, including plentiful raw material availability, low environmental impact, cost-effectiveness, improved safety, and high theoretical specific capacity[11-14]. These characteristics make iron-based materials suitable for both anode and cathode use in secondary batteries. Most energy storage mechanisms in iron-based electrode materials are based on conversion reactions, which have garnered considerable attention among transition metal compounds[15-18]. To date, numerous iron-based materials have been explored, including oxides, sulfides, selenides, phosphides, and fluorides [Figure 1]. Most of them possess high theoretical capacities exceeding 600 mAh g^{-1}[19-22]. Nevertheless, iron-based materials face inherent challenges, such as low electronic conductivity and sluggish ion diffusion, especially due to the large radius of Na^+ ions, thus causing poor rate capability and pronounced voltage hysteresis. In addition, massive volume expansion and the agglomeration of Fe^0 during charging/discharging compromise the structural integrity of the electrodes, resulting in poor cycle stability. To address these issues, researchers have developed various strategies, including nanostructure design, conductive coating or compositing, hierarchical porous structures, and electrolyte optimization[19-22]. For instance, Zhao *et al.* synthesized Fe_3O_4/PPy nanospheres via a hydrothermal method followed by ultrasonication-assisted polymerization[11]. The conductive polypyrrole (PPy) coating improved the conductivity, while the hollow porous structure enhanced structural stability[11]. Hou *et al.* In another example, FeP@C arrays supported on a conductive reduced graphene oxide network through a simple solution-phase reaction and gas-phase phosphidation[15]. These FeP@C arrays effectively mitigated volumetric strain, while the carbon coating enhanced electrical conductivity and prevented particle agglomeration during cycling[15]. Thus, the rational design of nanostructures and the development of straightforward synthesis methods are crucial to improving the electrochemical performance of conversion-type iron-based electrodes. This manuscript summarizes recent progress in iron-based electrodes for SIBs and outlines future research directions. It is hoped that this review could provide valuable insights for the development of high-performance iron-based electrodes in SIBs.

RECENT ADVANCES IN IRON-BASED ELECTRODES

Compared to the currently available cathodes/anodes for SIBs, iron-based electrodes offer several advantages: they are derived from plentiful resources, produce no pollution, are environmentally friendly,

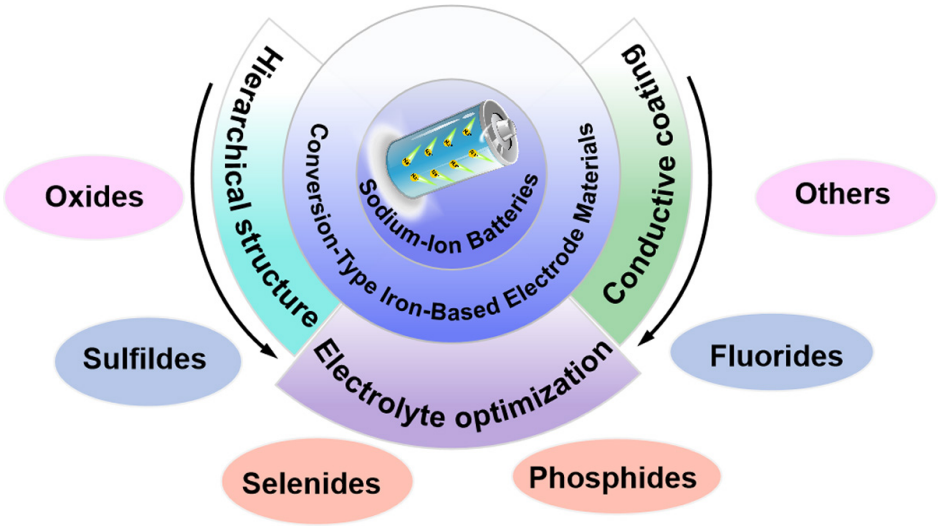

Figure 1. Schematic illustration of conversion-type iron-based materials for SIBs.

have low costs, ensure good safety profiles, and possess high theoretical specific capacity[11,15-17]. Consequently, these materials can be utilized as both cathodes/anodes in secondary batteries. The Na^+ storage mechanism of iron-based electrodes is mostly classified as conversion-type.

Iron-based oxides

In recent years, iron-based oxides have gradually become the most promising electrodes due to their ultrahigh theoretical capacities and abundant natural availability[11,17-21]. These oxides include FeO, Fe_3O_4, and Fe_2O_3, with Fe_2O_3 (theoretical specific capacity ~1,008 mA h g^{-1}) and Fe_3O_4 (926 mAh g^{-1}) being the most extensively studied[11,17]. The sodium-ion storage mechanism of Fe_2O_3 in SIBs is as follows[21-24]:

$$Fe_2O_3 + 2Na^+ + 2e^- \leftrightarrow Na_2Fe_2O_3 \quad (1)$$

$$Na_2Fe_2O_3 + 4Na^+ + 4e^- \leftrightarrow 3Na_2O + 2Fe \quad (2)$$

However, iron oxide electrodes suffer from several inherent shortcomings: (1) the generation of electrochemically inactive Na_2O during cycling severely degrades cycle stability; (2) the intrinsic low conductivity leads to sluggish ion diffusion, poor rate capability, and significant voltage hysteresis; (3) massive volume expansion and Fe^0 nanoparticle agglomeration during cycling cause structural damage and rapid capacity decay[17,22-24].

To overcome these challenges, researchers have designed various nanostructures and incorporated conductive coatings on iron-based materials to enhance electronic conductivity and structural integrity[15,17]. For instance, Li *et al.* designed a hierarchical Fe_2O_3@MIL-101(Fe)/C anode via a MOF-derived method[18]. The hierarchical nanostructure increases the surface areas, facilitating electrolyte infiltration and shortening diffusion lengths for both Na^+ ions and electrons[18]. Furthermore, the intrinsic hollow architecture helps mitigate volume changes during Na^+ insertion/extraction. As a result, Fe_2O_3@MIL-101(Fe)/C exhibits excellent cycling stability, delivering a capacity of 662 mAh g^{-1} over 200 cycles at 200 mA g^{-1} with 93.2% capacity retention[18].

Graphene, known for its ultrahigh surface area and exceptional electronic conductivity, is also a highly promising component in electrode design. Li *et al.* synthesized Fe_2O_3 nanoparticles embedded in N-doped graphene with internal micro-channels (Fe_2O_3@N-GIMC)[19]. The interconnected porous structure offers abundant active sites and efficient ion pathways, while also mitigating nanoparticle aggregation and pulverization. Consequently, Fe_2O_3@N-GIMC exhibits outstanding Na^+ storage performance, achieving a capacity of 308.9 mAh g^{-1} over 1,000 cycles and 200.8 mAh g^{-1} over 4,000 cycles at 1 A g^{-1}[19].

To alleviate the volumetric strain and enhance the electronic conductivity of Fe_2O_3 anodes, Chen *et al.* encapsulated a Fe_2O_3 core in N-doped carbon nanosphere shells (MFe_2O_3@N-HCNs) through a simple confined impregnation crystallization method [Figure 2A][20]. The as-obtained MFe_2O_3@N-HCNs not only possess a connected hierarchical structure that shortens the diffusion length, but also effectively accommodate the significant volumetric stress during Na^+ insertion/extraction [Figure 2B and C]. Figure 2D shows a lattice spacing of 0.20 nm, which corresponds to the (410) crystal plane of Fe_2O_3. As a result, the MFe_2O_3@N-HCNs exhibit outstanding rate capability, achieving specific capacities of 454, 360, 309, 257, and 201 mAh g^{-1} at current densities of 0.1 to 2 A g^{-1}, respectively [Figure 2E]. Additionally, Figure 2F demonstrates that the MFe_2O_3@N-HCNs anode maintains superior cycling stability, retaining a capacity of 417 mAh g^{-1} after 100 cycles at 0.1 A g^{-1}[20].

Reduced graphene oxide (rGO) offers significant electronic conductivity and a high surface area, making it a promising composite material. Li *et al.* synthesized a composite of amorphous Fe_2O_3/graphene nanosheets (Fe_2O_3@GNS) via a simple procedure[21]. They found that amorphous ultrafine Fe_2O_3 particles (~5 nm) were uniformly riveted onto the GNS via strong oxygen-bridge (C-O-Fe) bonds. This composite anode exhibited superior Na^+ storage performance compared to well-crystallized Fe_2O_3. Specifically, theFe_2O_3@GNS anode delivered a capacity of 440 mAh g^{-1} at 0.1 A g^{-1}, yielding an initial Coulombic efficiency (ICE) of 81.2%. Even at a high current density of 2 A g^{-1}, it retained a capacity of 219 mAh g^{-1}. The strong interactions between GNS and Fe_2O_3 not only provided abundant active sites and facilitated Na^+/electron diffusion but also mitigated volume changes during discharging/charging[21]. Furthermore, Li *et al.* prepared single-crystal Fe_2O_3 particles (~300 nm) uniformly distributed on rGO nanosheets (Fe_2O_3/rGO)[22]. When used as an anode for SIBs, this Fe_2O_3/rGO composite demonstrated an ICE of 71% and retained a capacity of 610 mAh g^{-1} at 0.05 A g^{-1}, with 82% retention after 100 cycles[22]. Bhar *et al.* developed a free-standing anode by embedding Fe_2O_3 nanoparticles within a carbon fiber (CF) network, effectively mitigating the conductivity and pulverization issues associated with Fe_2O_3[23]. Their Fe_2O_3-CF anode delivered a discharge capacity of 1,154 mAh g^{-1}, substantially higher than that of conventional Fe_2O_3 anodes (653 mAh g^{-1}), and demonstrated a capacity retention of 70% over 100 cycles[23]. Zhao *et al.* constructed Fe_2O_3 nanorods directly on carbon cloth via a simple hydrothermal strategy to develop a free-standing SIB anode[24]. These Fe_2O_3 nanorods achieved an impressive specific capacity retention of 119% after 100 cycles[24]. In another study, Shi *et al. in situ* synthesized amorphous Fe_2O_3 on N-doped carbon (NC) nanofibers to form a novel Fe_2O_3/NC anode[25]. This anode achieved a Na^+ storage capacity of 408 mAh g^{-1} over 350 cycles at 0.1 A g^{-1} and maintained 183 mAh g^{-1} at 3 A g^{-1}[25]. The outstanding electrochemical features of these free-standing anodes are related to the synergistic effects between the nanostructured Fe_2O_3 and the cross-connected carbon fiber network, which not only alleviates volumetric strain and provides more active storage sites, but also enhances the overall electrode conductivity, thereby accelerating Na^+/electron diffusion during cycling.

Except for Fe_2O_3, Fe_3O_4 possesses a high theoretical capacity of 926 mAh g^{-1}, along with advantages such as safety, non-toxicity, environmental friendliness, abundant availability, and low cost. These properties have attracted significant attention to Fe_3O_4 as a promising anode material for SIBs[26-30]. The Na^+ storage mechanism of Fe_3O_4 proceeds as follows[26-30]:

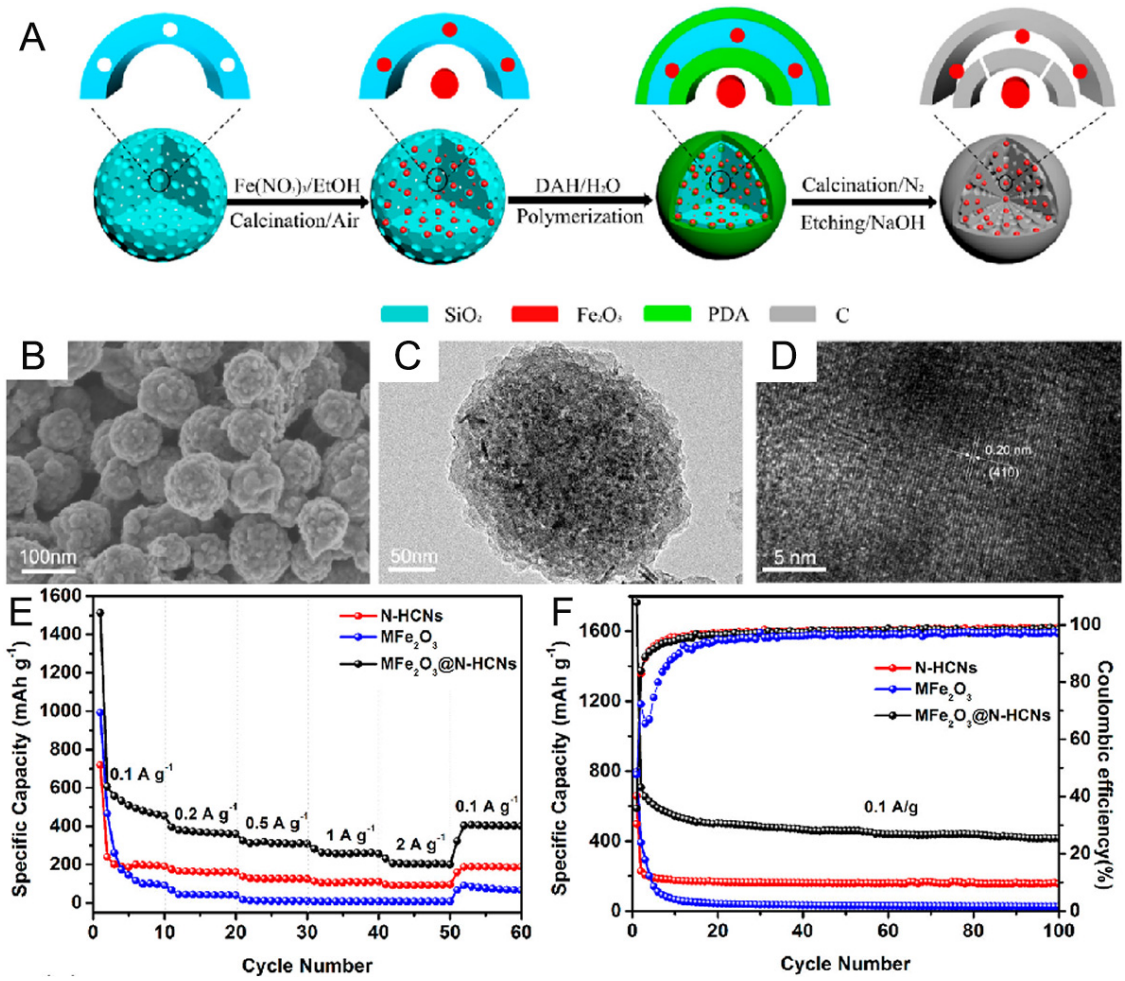

Figure 2. (A) Schematic diagram of the preparation process of MFe_2O_3@N-HCNs; (B) SEM, (C) TEM, and (D) HRTEM images of MFe_2O_3@N-HCNs. (E) Rate capabilities of N-HCNs, MFe_2O_3, and MFe_2O_3@N-HCNs anodes from 0.1 to 2 A g^{-1}; (F) Cycling performance of N-HCNs, MFe_2O_3, and MFe_2O_3@N-HCNs at 0.1 A g^{-1}[20]. Copyright 2021, American Chemical Society.

$$Fe_3O_4 + xNa^+ + xe^- \leftrightarrow Na_xFe_3O_4 \quad (3)$$

$$Na_xFe_3O_4 + (8\text{-}x)Na^+ + (8\text{-}x)e^- \leftrightarrow 4Na_2O + 3Fe \quad (4)$$

However, similar to other transition metal oxides, Fe_3O_4 suffers from substantial volume expansion during cycling. This volume change causes structural degradation and results in poor cycle stability, thereby limiting its practical application[27-31]. To address this challenge, Liu *et al.* synthesized a composite of graphene and Fe_3O_4 nanodots through a simple hydrothermal procedure and applied it as an anode material for SIBs[26]. This unique hierarchical structure provides a large solid electrolyte interphase (SEI) that facilitates rapid Na^+/electron diffusion, mitigates volumetric strain, and prevents aggregation of nano-Fe_3O_4 during discharging/charging. Consequently, the graphene-Fe_3O_4 quantum dot composite achieved a high specific capacity of 525 mAh g^{-1} at 0.03 A g^{-1} and exhibited excellent cycling stability, retaining 312 mAh g^{-1} after 200 cycles at 50 mA g^{-1}[26]. To further overcome the low conductivity of Fe_3O_4, Tao *et al.* developed an N/S/P-doped dual carbon-modified Fe_3O_4 nanoparticle (Fe_3O_4@C@G)[27]. As illustrated in Figure 3A, the N/S/P-doped carbon shell was formed by pyrolyzing a multi-heteroatom-containing polymer, resulting in a core-shell Fe_3O_4@C structure, which was subsequently encapsulated with rGO to form Fe_3O_4@C@G[27]. SEM

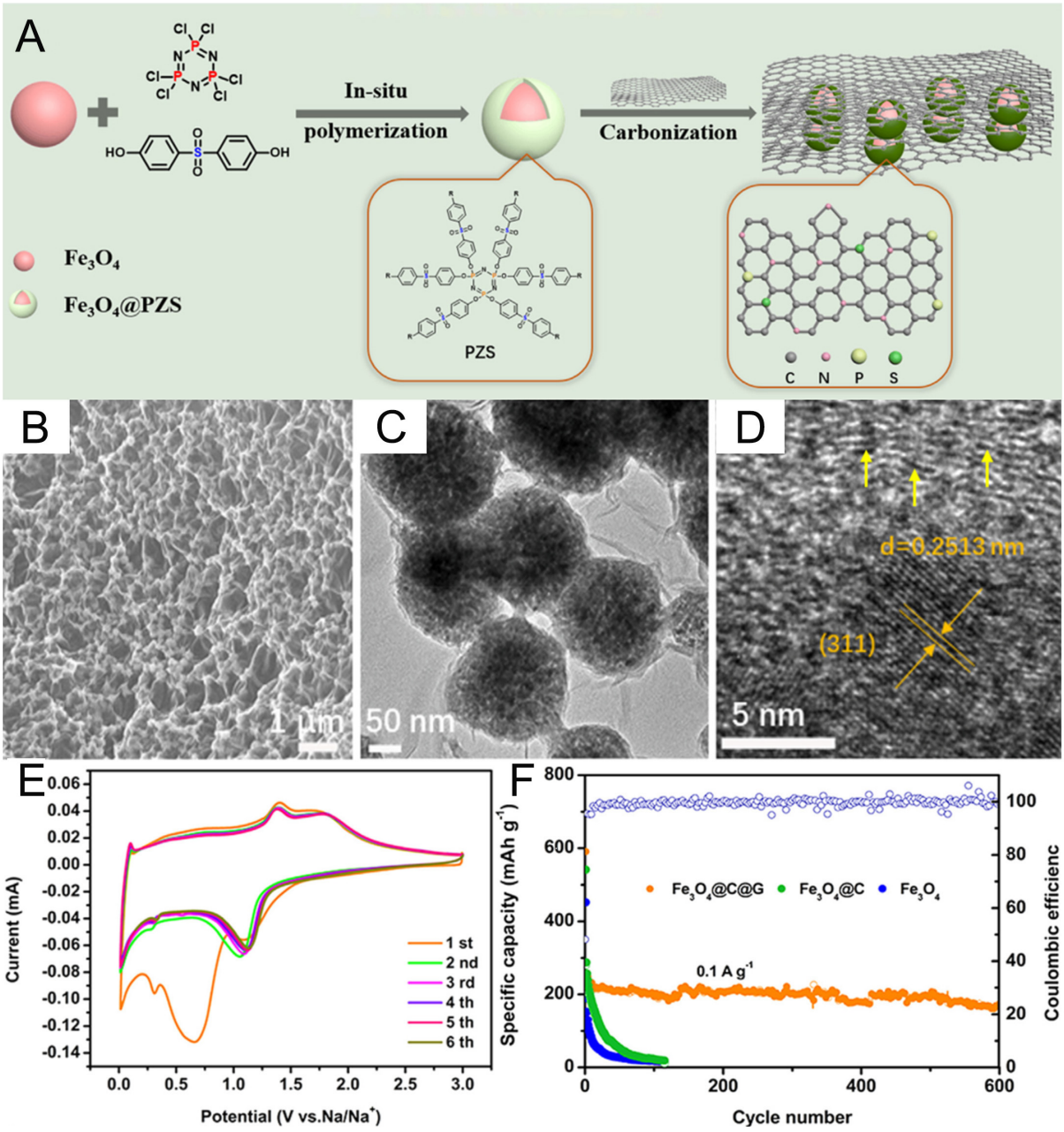

Figure 3. (A) Schematic illustration of the preparation of Fe_3O_4@C@G. (B) SEM, (C) TEM, and (D) HRTEM images of Fe_3O_4@C@G. (E) CV curves of Fe_3O_4@C@G; (F) Comparison of the cycling performance of Fe_3O_4, Fe_3O_4@C, and Fe_3O_4@C@G at 0.1 A g^{-1} [27]. Copyright 2020, Elsevier.

images [Figure 3B] show that numerous nanospheres are uniformly distributed on the rGO layers. TEM images [Figure 3C and D] further confirm that Fe_3O_4 nanoparticles with carbon shells are wrapped by rGO. The initial six CV curves of Fe_3O_4@C@G [Figure 3E] show broad cathodic/anodic peaks within the ranges of 1.0~1.25 and 1.25~1.5 V, respectively, corresponding to the reversible redox reactions described in Eq. 2. From the second cycle onward, the CV curves largely overlap, suggesting excellent electrochemical reversibility of the Fe_3O_4@C@G anode. When applied as an anode for SIBs, Fe_3O_4@C@G delivered a capacity of 180 mAh g^{-1} over 600 cycles at 0.1 A g^{-1} [Figure 3F][27]. Biswal *et al.* synthesized a dual core@shell Fe_3O_4@C@polypyrrole (PPy) composite anode[28]. This material showed a capacity of 64 mAh g^{-1} over

100 cycles at 0.1 A g^{-1}[28].

Conventional carbon coating strategies primarily enhance electrical conductivity and mitigate volume expansion at the macro scale. In contrast, metal-organic framework (MOF)-derived approaches have emerged as effective nanoscale engineering methods, enabling the *in situ* encapsulation of metal oxide quantum dots during pyrolysis[29]. Qi *et al.* developed Fe_3O_4 quantum dots embedded in a raspberry-like carbon framework (Fe_3O_4 QD@C-GN) using iron-based MIL-88-Fe-NH_2 as a template[29]. When tested within the voltage range of 0.05~3.0 V, Fe_3O_4 QD@C-GN exhibited capacities of 343, 234, and 149 mAh g^{-1} at 2, 5 and 10 A g^{-1}, respectively, over 1,000 cycles[29].

To address the issues of poor electronic conductivity and structural degradation induced by the high volume stress during cycling, Qin *et al.* creatively introduced a magnetic stimulus to increase pressure within the sample chamber. This approach facilitated the uniform deposition of red P particles onto a chain-like Fe_3O_4/C composite, forming Fe_3O_4/C/P. When used as an anode material and cycled within a voltage range of 0.01~3 V, the Fe_3O_4/C/P structure exhibited excellent cycling stability and outstanding rate capability[30]. This magnetic field-assisted strategy effectively bridges the synthesis method with enhancements in electrochemical properties. Huang *et al.* encapsulated Fe_3O_4 in N-doped carbon nanofibers (CFs) through an electrospinning strategy followed by high-temperature calcination. The resulting three-dimensional (3D) interconnected CF network enhanced overall electronic conductivity, while N-doping introduced additional sites for Na^+ storage. Hence, the optimized Fe_3O_4-CFs achieved a considerable capacity of 358.1 mAh g^{-1} over 200 cycles at 0.5 A g^{-1}[31].

Although structural regulation, composite modification, and surface engineering have markedly improved the electrochemical performance of iron-based oxides for SIBs, further enhancements are still required to meet the demands of practical applications.

Iron-based sulfides

Compared to Na_2O, Na_2S exhibits higher electrochemical reactivity, and iron-based sulfide materials have also attracted considerable attention[20,31-34]. These materials offer relatively high theoretical capacities and are composed of naturally abundant, non-toxic and cost-effective elements (e.g., Fe and S)[35-39]. To date, a series of iron-based sulfides have been explored. Among them, FeS_2 has received particular attention due to its ultrahigh capacity of 894 mAh g^{-1} resulting from a four-electron/Na^+ transfer per FeS_2 unit. Kitajou *et al.* investigated the discharge/charge mechanism of FeS_2 using synchrotron-based X-ray adsorption near-edge structure (XANES), X-ray photoelectron spectroscopy (XPS), and X-ray diffraction (XRD)[32]. The Na^+ storage process in FeS_2 proceeds as follows[32-35]:

$$FeS_2 + 2Na^+ + 2e^- \leftrightarrow Na_2FeS_2 \quad (5)$$

$$Na_2FeS_2 + 2Na^+ + 2e^- \leftrightarrow Fe + 2Na_2S \quad (6)$$

The main contributors to the irreversible capacity are (i) the dissolution of S_2^{2-} ions during charging/discharging; and (ii) the inevitable formation of a SEI layer, both of which result in low ICE[36-40]. To address these challenges, strategies such as nanochemistry, structural regulation, and surface modification have proven effective[39-42]. For instance, Li *et al.* demonstrated through *ex situ* TEM measurements that only a portion of FeS_2 actively participates in the conversion reaction, while the formation of "inactive cores" leads to low capacity[33]. Moreover, the sluggish diffusion kinetics induced by the relatively larger Na^+ ionic radius exacerbate electrode pulverization, thereby causing rapid capacity decay[33]. Zhang *et al.* developed

mesoporous FeS_2 nanorods via a scalable synthesis method[34]. Due to their unique one-dimensional porous structure and excellent strain relaxation capabilities, these nanorod anodes exhibited outstanding Na^+ storage performance, maintaining a reversible capacity of 711.1 mAh g^{-1} over 450 cycles at 1 A g^{-1}[34].

Despite the high theoretical capacity of FeS_2, its practical application remains limited due to severe volume fluctuations during charging/discharging and the formation of soluble polysulfides at low voltages (< 0.8 V *vs.* Na/Na^+). Kandula *et al.* designed N-doped carbon-coated FeS_2 nanoparticles wrapped in N/S co-doped graphene/single-walled carbon nanotubes (FSCGS) via hydrothermal sulfuration[35]. When used as an anode for SIBs, the FSCGS composite achieved a superior rate capability (476 mAh g^{-1} at 10.0 A g^{-1}). Furthermore, it demonstrated excellent stability with a capacity retention of 91.3% over 200 cycles at 0.5 A g^{-1}[35]. The superior performance is attributed to the enhanced electron conductivity and electrochemical reactivity provided by the dual-carbon-modified hierarchical structure. Ma *et al.* designed a core-shell hollow sphere FeS_2 (CHS-FeS_2) using MIL-88B(Fe) as a template[36]. Its unique porous structure provides ample void space to buffer volume strain and promote Na^+ diffusion. As a result, the CHS-FeS_2 anode maintained a capacity of 546.5 mAh g^{-1} over 100 cycles at 0.5 A g^{-1} and retained 224 mAh g^{-1} even at 20 A g^{-1}, reflecting its remarkable Na^+ storage performance[36]. Lu *et al.* embedded ultrafine FeS_2 particles into N/S co-doped CFs, along with FeS_2 nanoflakes, forming a composite (FeS_2@CF-NS) via electrospinning followed by annealing[37]. This unique architecture effectively reduces the Na^+ diffusion path, accelerates Na^+/e^- diffusion, and mitigates volume strain during discharging/charging. The FeS_2@CF-NS composite demonstrated a high specific capacity of 637.1 mAh g^{-1} after 400 cycles at 1 A g^{-1} and retained 431.1 mAh g^{-1} at 5 A g^{-1}[37]. Ma *et al.* synthesized a series of $Co_xFe_{1-x}S_2$ compounds with varying Co content via a typical solvothermal sulfuration procedure[36]. Among them, the optimized $Co_{0.5}Fe_{0.5}S_2$ delivered a capacity of 220 mAh g^{-1} over 5,000 cycles at 2 A g^{-1}, and 172 mAh g^{-1} even at 20 A g^{-1}. Structural analysis revealed the formation of layered $Na_xCo_{0.5}Fe_{0.5}S_2$ during the initial discharging, which was preserved in subsequent cycles[38]. Man *et al.* fabricated a yolk-shell FeS_2@C anode for SIBs[39]. The porous yolk-shell design not only facilitates rapid Na^+/e^- diffusion but also buffers the large volume changes of FeS_2 during Na^+ insertion/extraction. The as-prepared FeS_2@C achieved a reversible capacity of 616 mAh g^{-1} over 100 cycles at 0.1 A g^{-1}[39]. Liu *et al.* developed novel yolk-shell FeS_2@C nanoboxes using a facile etching procedure combined with a unique sulfidation-in-nanobox strategy[40]. These nanoboxes displayed remarkable electrochemical properties, achieving a specific capacity of 330 mAh g^{-1} over 800 cycles at 2 A g^{-1}[40].

Furthermore, Xu's group successfully prepared pitaya-like FeS_2@C via a one-step *in-situ* encapsulation and hydrothermal sulfuration strategy, with ferrocene serving as both the iron and carbon source [Figure 4A][41]. FeS_2 particles are uniformly embedded in the porous carbon matrix, effectively preventing the agglomeration of Fe^0 nanoparticles and minimizing the dissolution of S_2^{2-}. Furthermore, the porous structure facilitates Na^+ ion diffusion, significantly improving the electrochemical performance of FeS_2. As depicted in Figure 4B, the pitaya-structured FeS_2@C exhibits an initial discharge/charge capacity of ~701/579 mAh g^{-1} at 0.1 A g^{-1}. It maintains a capacity of 415 mAh g^{-1} over 100 cycles at 0.6 A g^{-1} [Figure 4C]. Figure 4D and E illustrates that FeS_2@C delivers stable reversible Na^+ storage capabilities of 580, 502, 463, 422, 374, and 307 mAh g^{-1} at current densities ranging from 0.1 to 3.2 A g^{-1}, respectively[41]. Such excellent Na^+ storage performance benefits from the porous carbon sphere framework, which effectively suppresses the shuttle effect of S_n^{2-} ions and contributes to excellent cycling stability. Simultaneously, the porous carbon matrix enhances the overall conductivity of the material. Furthermore, it acts as a flexible buffer, accommodating volume changes during Na^+ insertion/extraction and thereby preserving the structural integrity of the electrode.

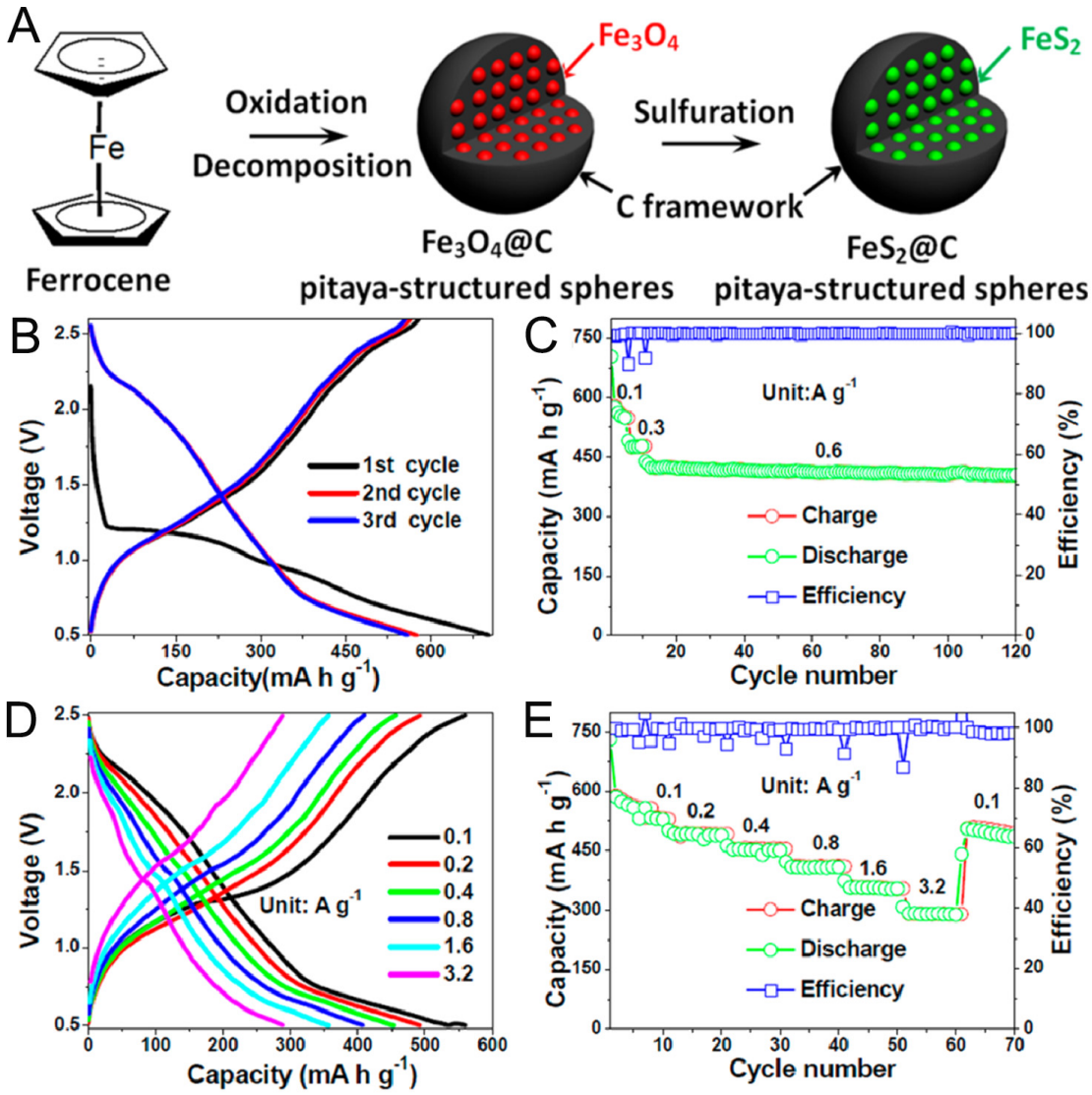

Figure 4. (A) Schematic illustration of the preparation process for pitaya-structured FeS_2@C. (B-E) electrochemical performance of FeS_2@C: (B) initial three charge/discharge profiles, (C) cycling performance at 0.6 A g^{-1}, (D) charge/discharge profiles from 0.1, 0.2, 0.4, 0.8, 1.6 to 3.2 A g^{-1}, respectively, (E) rate performance[41]. Copyright 2017, American Chemical Society.

Chen *et al.* encapsulated graphene-coated FeS_2 in carbon nanofibers using an electrospinning strategy and employed it as an anode for SIBs[42]. The double carbon modification improved electrical conductivity, thereby improving the structural reversibility of FeS_2 during desodiation/sodiation; thus, the material maintained a high capacity of 305.5 mAh g^{-1} over 2,450 cycles at 3 A g^{-1}. Owing to the markedly enhanced conductivity of the graphene-encapsulated FeS_2 nanoparticles, the composite also exhibited excellent temperature tolerance, retaining stable capacity performance at 0 °C and -20 °C. When paired with $Na_3V_2(PO_4)_3$ in full-cell configurations, the system delivered reversible capacities of 95, 50, and 43 mAh g^{-1} at room temperature, 0 °C, and -20 °C, respectively. Density functional theory calculations further revealed that dual carbon modification effectively reduces the Na^+ diffusion barrier and facilitates reversible Na^+ storage[42].

FeS also possesses a high theoretical specific capacity (~609 mAh g^{-1}) and has been widely explored as an anode material for SIBs[43,44]. Its Na^+ storage mechanism involves a two-step conversion reaction, as described below[45-49]:

$$FeS + xNa^+ + xe^- \rightarrow Na_xNaS\ (0 < x < 2) \quad (7)$$

$$Na_xFeS + (2\text{-}x)Na^+ + (2\text{-}x)e^- \rightarrow Fe + Na_2S \quad (8)$$

FeS also suffers from unsatisfactory electrical conductivity and significant volumetric strain leading to rapid capacity decay and poor rate performance[43,49]. To address these issues, Cho *et al.* fabricated yolk-shell structured FeS/C composites via a vapor-pressure-induced synthesis route[43]. The ultrathin carbon coatings on the FeS nanosheets effectively improved their electrical conductivity and mitigated the volumetric strain during sodiation. As a result, the FeS/C yolk-shell nanosheets delivered a reversible capacity of 300.4 mAh g^{-1} over 10,000 cycles, with 81.1% capacity retention at 10 A g^{-1}[43]. Han *et al.* prepared porous FeS nanofiber anodes for SIBs via electrospinning followed by sulfidation[44]. During synthesis, ultrafine Fe_2O_3 nanocrystals diffused to the fiber surface through Ostwald ripening and then transferred into porous FeS sulfidation. The resulting FeS nanofibers featured abundant nanovoids that help buffer volumetric strain and maintain structural stability, thereby enabling excellent Na^+ storage properties. These nanofibers exhibited an initial discharge capacity of 561 mAh g^{-1} and maintained 592 mAh g^{-1} at 0.5 A g^{-1} over 150 cycles. When cycled at increasing current densities from 0.2 to 5.0 A g^{-1}, the FeS anode retained capacities of 456, 437, 413, 394, 380, and 353 mAh g^{-1}, respectively[44]. Liu *et al.* synthesized a FeS/NC composite via an *in situ* chemical transformation method[45]. In this design, FeS nanocrystals were encapsulated by the *in-situ* generated N-doped carbon (NC) matrix. The FeS/NC anode exhibited a high charge capacity of 511 mAh g^{-1} over 100 cycles at 0.2 A g^{-1}, and retained 326 mAh g^{-1} after 500 cycles at 1.0 A g^{-1}. These excellent electrochemical results are ascribed to the NC matrix, which enhances electrical conductivity and accommodates the volume changes of FeS during Na^+ insertion/extraction[45]. Chen *et al.* developed a Mn-doped FeS/NC composite through a one-pot solvothermal reaction followed by thermal treatment[46]. Mn doping improved electrical conductivity, facilitated charge carrier transport, and expanded lattice spacing to promote Na^+ diffusion. The Mn-doped FeS/NC anode achieved a specific capacity of 563.3 mAh g^{-1} at 0.5 A g^{-1}, maintained 442.8 mAh g^{-1} at 8 A g^{-1}, and retained 206.2 mAh g^{-1} over 8,000 cycles[46].

The practical application of FeS anodes is hindered by their poor electronic conductivity and significant volume changes during cycling. Yuan *et al.* synthesized ultrafine FeS nanoparticles encapsulated in three-dimensional (3D) NC nanosheets using a facile sol-gel approach followed by a solid-state sulfidation process [Figure 5A][47]. As displayed in Figure 5B, the sol-gel-derived precursor forms a 3D cross-linked carbon framework upon thermal treatment. After sulfidation, FeS nanoparticles are uniformly embedded in the carbon nanosheets [Figure 5C and D]. When used as an anode material for SIBs, the 3D FeS@NC composite delivered a stable capacity of 254 mAh g^{-1} over 1,100 cycles at 1.5 A g^{-1} [Figure 5E][47]. These remarkable electrochemical features are associated with the 3D porous nanosheet structure, which dramatically enhances electronic conductivity, suppresses the pulverization and aggregation of FeS particles, immobilizes dissolved polysulfides, increases the electrolyte-electrode contact area, and provides abundant active sites for Na^+ storage.

The incompatibility between electrodes and electrolytes significantly limits the electrochemical performance of iron-based sulfides. Poor interfacial compatibility leads to unstable solid electrolyte interphase (SEI), resulting in persistent irreversible side reactions that consume active Na^+ ions. On account of these, Zhang *et al.* synthesized FeS@N,S-C, comprising spindle-structured FeS nanoparticles wrapped in N,S-

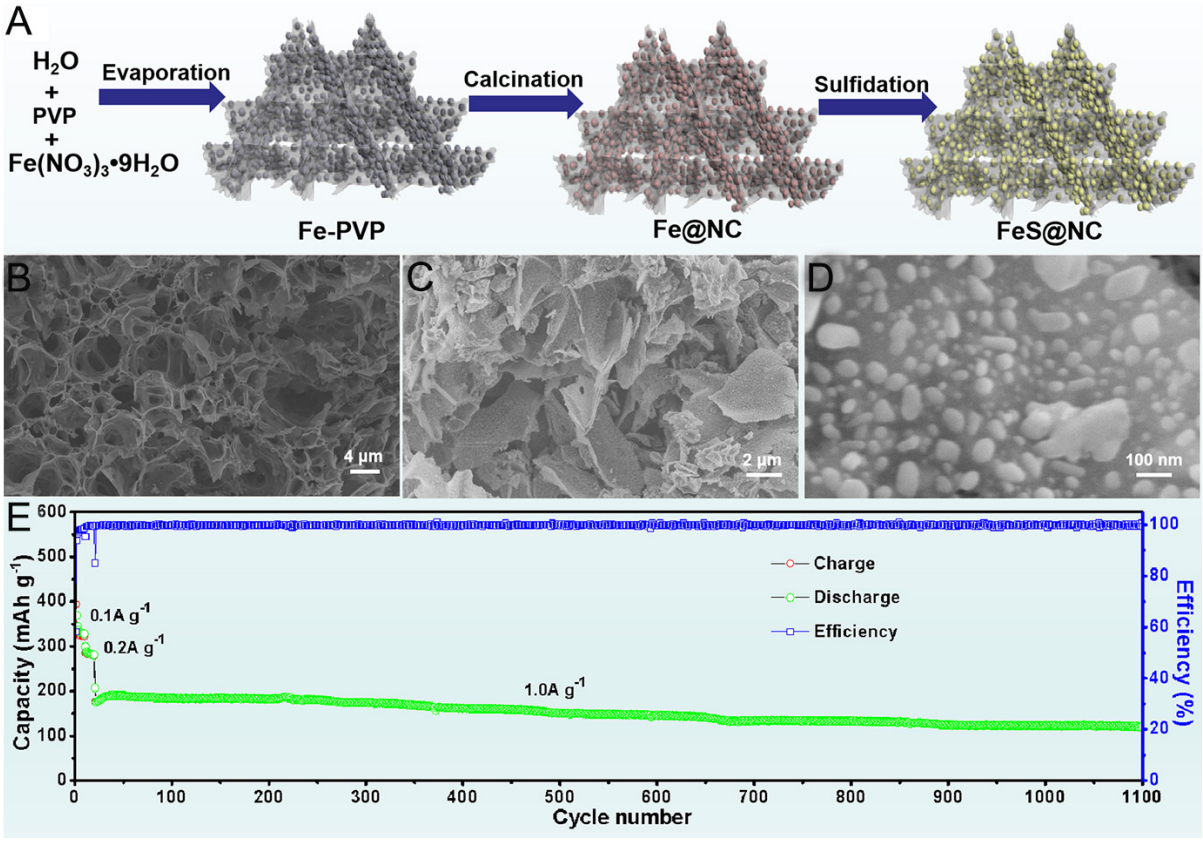

Figure 5. (A) Schematic of the preparation of FeS@NC. (B) SEM image of Fe@NC; (C and D) SEM images of FeS@NC, (E) long-term cycling performance of FeS@NC at 1.0 A g^{-1} [47]. Copyright 2022, Elsevier.

doped carbon, as an anode material for SIBs[48]. They investigated the interfacial stability in an ester-based electrolyte (1 M $NaClO_4$ in propylene carbonate/ethylene carbonate with 5% fluoroethylene carbonate). The Na//FeS@N,S-C half-cell demonstrated a long cycling lifespan of 294 days. Furthermore, the corresponding pouch cell displayed excellent cyclability, retaining 82.2% of its capacity over 170 cycles at 0.2 A g^{-1}. Their findings suggest that the N,S-doped coating layer preferentially adsorbs ClO_4^- ions, inducing strong repulsion toward solvated Na^+ ions and creating an anion-rich inner Helmholtz plane. This results in the formation of an inorganic species-rich SEI (mainly NaCl and Na_2O), which preserves the electrode's structural integrity[46].

Considering the challenges posed by dissolved polysulfides and significant volume expansion, Huang *et al.* synthesized a bubble film-like FeS/C composite using $Fe(NO_3)_3{\cdot}9H_2O$, sulfur, and polyvinylpyrrolidone as precursors, followed by freeze-drying and carbonization[49]. The bubble film-like FeS/C exhibited reversible Na^+ storage capacities of 455, 439, 405, 318, 256, and 219 mA h g^{-1} at current densities ranging from 0.1 to 5.0 A g^{-1}, respectively[49]. The superior electrochemical performance is mainly attributed to the porous bubble film-like structure, which effectively suppresses the agglomeration of active nanoparticles, thereby enhancing cycling stability. Additionally, the porous carbon framework improves overall electrical conductivity, enabling excellent rate capability and high capacity retention. Moreover, the porous structure provides ample void space that mitigates volume expansion and maintains the structural integrity during charging/discharging.

Iron-based selenides

The SEI formed during electrochemical reactions can hinder the transport of Na^+ ions, resulting in the low practical capacity of oxide-based anodes for SIBs[48-61]. As for sulfides, the formation of soluble polysulfide intermediates induces a "shuttle effect", which aggravates capacity decay[50-54]. In contrast, metal selenides exhibit relatively high electronic conductivity and energy conversion efficiency, making them promising electrode materials for SIBs[55-59]. Among the various selenides studied to date, $FeSe_2$ and Fe_7Se_8 are two of the most representative anode materials[58-61]. The Na-ion storage mechanism of $FeSe_2$ is as follows[58-63]:

$$FeSe_2 + xNa^+ + xe^- \leftrightarrow Na_xFeSe_2\ (0 < x < 2) \quad (9)$$

$$Na_xFeSe_2 + (4\text{-}x)Na^+ + (4\text{-}x)e^- \leftrightarrow Fe + Na_2Se \quad (10)$$

However, the sluggish diffusion kinetics and severe volume expansion during cycling lead to rapid capacity fading, hampering the practical application of $FeSe_2$ in SIBs. Wei *et al.* synthesized nanorod-assembled $FeSe_2$ clusters via a hydrothermal strategy and investigated their Na^+ storage performance under various electrolyte conditions[50]. When paired with an ether-based electrolyte, the $FeSe_2$ clusters demonstrated superior electrochemical properties, delivering a high capacity of 515 mAh g^{-1} over 400 cycles at 1 A g^{-1} and a high ICE of 97.4%. Remarkably, they retained 128 mAh g^{-1} even at an ultrahigh current density of 35 A g^{-1}[50]. Additionally, Wang *et al.* prepared NC-encapsulated $FeSe_2$ (NC-$FeSe_2$) with a controlled porous structure using a straightforward salt template-assisted strategy[51]. As an SIB anode, NC-$FeSe_2$ achieved a reversible capacity of 520.4 mA h g^{-1} over 100 cycles at 1 A g^{-1}. Even at 10 A g^{-1}, it maintained a capacity of 333 mAh g^{-1} over 1,800 cycles, demonstrating exceptional long-cycle stability. The high ICE (78.9 %) and excellent diffusion kinetics are ascribed to its hierarchical porous structure and intrinsic pseudocapacitive behaviors[51]. Park *et al.* synthesized a $FeSe_2$-amorphous carbon ($FeSe_2$-AC) composite anode for SIBs via a large-scale spray-drying strategy [Figure 6A][52]. As displayed in Figure 6B and C, ultrafine $FeSe_2$ nanoparticles are uniformly embedded in AC microspheres formed from a 30 g L^{-1} dextrin spray solution. TEM images in Figure 6D and E reveal that the $FeSe_2$ crystals (< 20 nm) are homogeneously distributed within the carbon matrix. As shown in Figure 6F, increasing the dextrin concentration from 0, 10, 20 to 30 g L^{-1} resulted in progressively improved discharge capacities of 85, 194, 203, 379 mAh g^{-1} over 150th cycles at 0.5 A g^{-1}, respectively. The optimized $FeSe_2$-AC composite achieved stable reversible capacities of 431, 399, 375, 346, 326, 309, and 286 mA h g^{-1} at current densities ranging from 0.2 to 5 A g^{-1} [Figure 6G][52].

Li *et al.* discovered that surface oxides significantly affect the electrochemical activity of $FeSe_2$[53]. $FeSe_2$ with a larger size and lower oxide content demonstrated superior properties compared to $FeSe_2$/graphene composites with higher oxide content. By modulating the oxide content of the $FeSe_2$/graphene anode, a specific capacity of 459 mAh g^{-1} was retained at 0.1 A g^{-1}. This composite also displayed excellent rate capability, with only a 10% capacity loss when the current density increased from 0.1 to 5 A g^{-1}. Remarkably, the $FeSe_2$/graphene maintained a capacity of 227 mAh g^{-1} over 800 cycles even at 25 A g^{-1}[53]. The surface oxide was found to transform into a sodiated shell with poor conductivity and high mechanical strength, which induced phase-transfer resistance. This resistance hindered the sodiation of the $FeSe_2$ core and impeded the diffusion of Na^+/electrons during subsequent sodiation processes. Zheng *et al.* reported that $FeSe_2$@NC micro rods, consisting of a $FeSe_2$ core and a NC shell with ample void space, were adopted as anodes for SIBs[53]. This ingeniously designed porous core-shell structure enhanced Na^+/electron transport, prevented $FeSe_2$ degradation from electrolyte exposure, and accommodated volume changes due to sufficient void space. As a result, the $FeSe_2$@NC microrods achieved outstanding Na^+ storage performance, maintaining a capacity of 411 mAh g^{-1} at 10.0 A g^{-1} and 401.3 mAh g^{-1} over 2,000 cycles at 5.0 A g^{-1}[53].

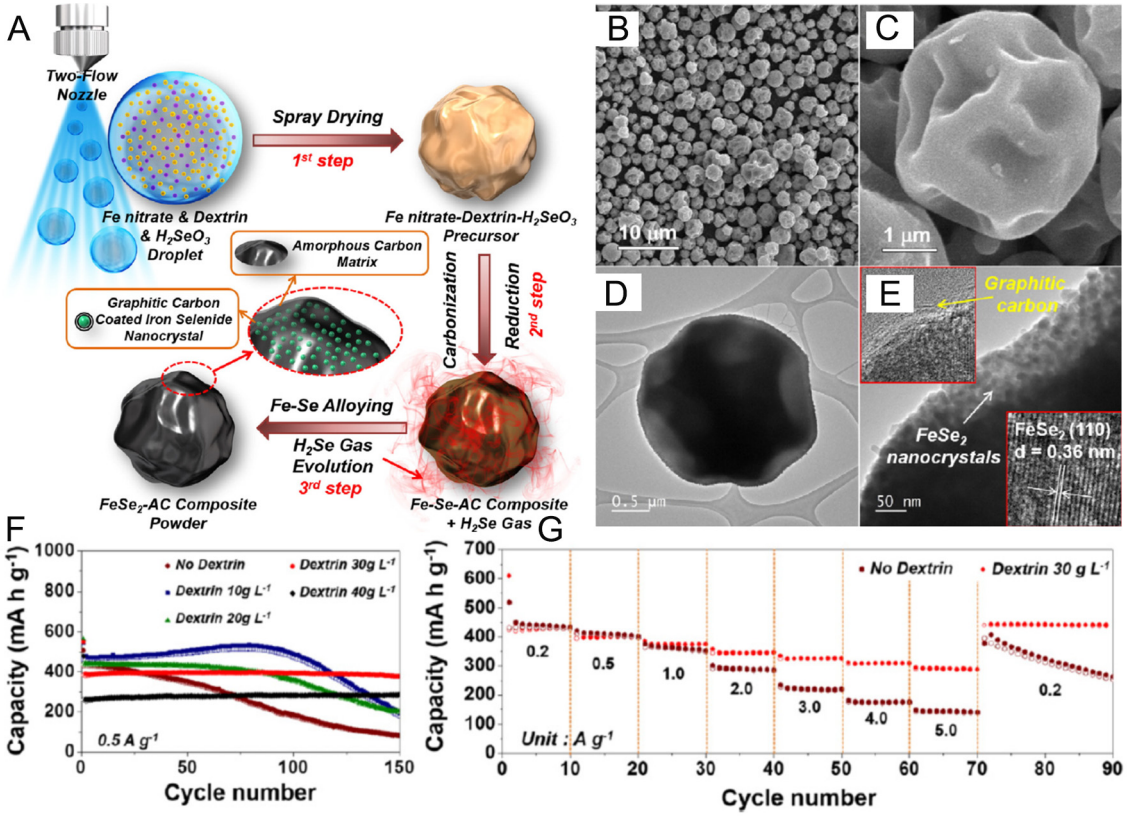

Figure 6. (A) Schematic illustration of the preparation process of the $FeSe_2$-AC composite powder by the spray drying process, (B and C) SEM images and (D and E) TEM images of $FeSe_2$-AC; (F) cycling performance of $FeSe_2$-AC at 0.5 A g^{-1}; (G) cycling performance of $FeSe_2$-AC at 0.5 A g^{-1} [52]. Copyright 2020, Elsevier.

To maintain structural integrity during cycling, Pan *et al.* proposed a $FeSe_2$@NC composite anode. The strong interaction between $FeSe_2$ nanorods and NC facilitates fast interfacial Na^+/e^- diffusion and enhances structural stability[54]. As a result, the $FeSe_2$@NC electrode exhibited a capacity of 379.2 mA h g^{-1} at a high current density of 10 A g^{-1}. When paired with a $Na_3V_2(PO_4)_2F_3$@reduced graphene oxide cathode, the full cell achieved 167.2 mAh g^{-1} at 1 A g^{-1} over 1,000 cycles[54]. Zhou *et al.* synthesized a porous NC framework (NCF) embedded with $FeSe_2$ (P-$FeSe_2$/NCF) via a spray-drying and salt-template strategy[55]. This unique structure facilitates Na^+/electron transport and alleviates large volume changes during cycling. As an anode for SIBs, P-$FeSe_2$/NCF delivered 507 mAh g^{-1} over 200 cycles at 2 A g^{-1} and retained 386.7 mAh g^{-1} over 500 cycles at 10 A g^{-1}[55]. Men *et al.* fabricated a CNT/$FeSe_2$/C composite by encapsulating $FeSe_2$/C within a carbon nanotube (CNT) framework through a facile wet-chemistry procedure followed by selenization[56]. The resulting three-dimensional network enhanced electronic/ionic transport while providing void space to accommodate volume expansion. The CNT/$FeSe_2$/C composite exhibited excellent Na^+ storage performance, delivering 546 mAh g^{-1} over 100 cycles at 0.1 A g^{-1}. Even at a high mass loading of 16.9 mg cm^{-2}, it achieved impressive volumetric and areal capacities of 158 mAh cm^{-3} and 5.06 mAh cm^{-2}, respectively[56]. Furthermore, Yousaf *et al.* developed a $FeSe_2$-HGCNS composite using hollow graphitic carbon nanoshells, prepared via a spray granulation approach followed by selenidation[57]. Benefiting from its distinctive 3D structure, the $FeSe_2$-HGCNS electrode maintained a capacity of 425 mAh g^{-1} at 0.5 A g^{-1} over 100 cycles[57].

The sodium storage mechanism of Fe_7Se_8 proceeds through the following electrochemical reactions during discharging[58-63]:

$$Fe_7Se_8 + xNa^+ + xe^- \rightarrow Na_xFe_7Se_8 \quad (11)$$

$$Na_xFe_7Se_8 + yNa^+ + ye- \rightarrow Na_{x+y}FeSe_2 + 6FeSe \quad (12)$$

$$Na_{x+y}FeSe_2 + (4-x-y)Na^+ + (4-x-y)e^- \rightarrow 2Na_2Se + Fe \quad (13)$$

$$FeSe + 2Na^+ + 2e^- \rightarrow Na_2Se + Fe \quad (14)$$

The corresponding charging reactions are as follows:

$$Fe + 2Na_2Se \rightarrow Na_xFeSe_2 + (4-x)Na^+ + (4-x)e^- \quad (15)$$

$$3Fe + 4Na_xFeSe_2 \rightarrow Fe_7Se_8 + 4xNa^+ + 4xe^- \quad (16)$$

Tian *et al.* fabricated a monolithic architecture composed of radially aligned Fe_7Se_8 nanorod bundles (Fe_7Se_8 NRBs) using a facile self-template strategy followed by annealing[58]. The Fe_7Se_8 NRB anode delivered a specific capacity of 300 mAh g^{-1} at 0.5 A g^{-1} and retained 190 mAh g^{-1} over 8,000 cycles at a high current density of 20 A g^{-1}, indicating prominent long-cycling stability. This feasible strategy highlights the potential of structural engineering to enhance the electrochemical performance of selenide-based materials[58]. Liu *et al.* developed a one-step pyrolysis strategy to prepare metal chalcogenide materials[59]. The obtained carbon-coated Fe_7Se_8@C nanorods exhibited specific capacities of 442.4, 409.0, 393.8, 372.0, 365.3, and 353.8 mAh g^{-1} at 442.4, 409.0, 393.8, 372, 365.3, and 353.8 mAh g^{-1}, respectively. The remarkable rate performance of the Fe_7Se_8@C anode is attributed to the carbon coating, which enhances overall conductivity and mitigates volume expansion during charging/discharging. To further address volumetric strain and improve structural stability, Chen *et al.* proposed an innovative stress release strategy by encapsulating yolk-shell Fe_7Se_8@C structures with $MoSe_2$ nanosheets[60]. Due to its unique microstructure, the Fe_7Se_8@C@$MoSe_2$ composite exhibited an irreversible capacity of 473.3 mAh g^{-1} at 0.1 A g^{-1}, maintained 274.5 mAh g^{-1} at 5.0 A g^{-1}, and demonstrated 87.1% capacity retention over 600 cycles at 1.0 A g^{-1}. Chen *et al.* synthesized core-shell Fe_7Se_8 nanorods (Fe_7Se_8@NC) through an *in-situ* self-polymerization followed by a carbonization-selenization process[60]. The resulting Fe_7Se_8@NC electrode maintained a capacity of 290.7 mAh g^{-1} at 10 A g^{-1} and exhibited 84.6 % capacity retention over 6,000 cycles at 5 A g^{-1}[60]. The core-shell configuration significantly enhanced Na^+ diffusion and minimized irreversible side reactions, effectively accommodating volume changes and preserving structural integrity. Yuan *et al.* synthesized Fe_7Se_8@C nanotubes using Fe_2O_3 as the precursor and Fe_3O_4@C as a sacrificial template [Figure 7A][61]. As displayed in Figure 7B-D, the resulting Fe_7Se_8@C structures successfully retained the nanotube morphology of both the Fe_2O_3 precursor and Fe_3O_4@C intermediate. Utilized as an anode for SIBs, the Fe_7Se_8@C nanotubes demonstrated a capacity of 319 mAh g^{-1} over 720 cycles at 2 A g^{-1} [Figure 7E]. The excellent electrochemical performance is attributed to the hierarchical nanotube structure, which alleviates volume strain and provides efficient Na^+/electron transport channels. Additionally, the NC shell enhances overall conductivity and helps maintain electrode integrity during cycling[61,62].

Yang *et al.* developed Fe_7Se_8@NC nanoboxes (Fe_7Se_8@NC NBs) by fully encapsulating Fe7Se8 within a robust NC shell via a facile etching and selenization process[63]. As an anode material for SIBs, the Fe_7Se_8@NC NBs reached a Na^+ storage capacity of 385.5 mAh g^{-1} at 0.1 A g^{-1} and maintained 345.2 mAh g^{-1}

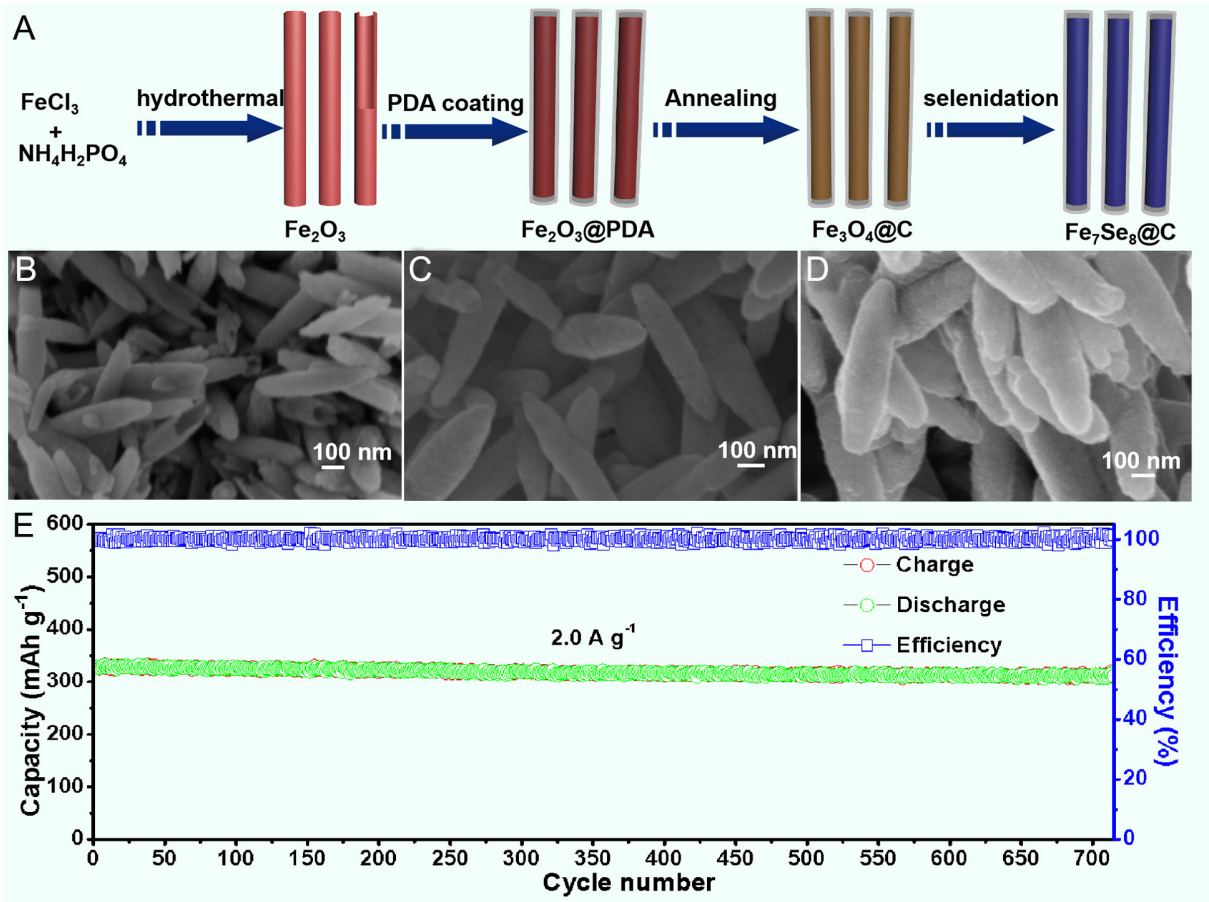

Figure 7. (A) Schematic illustration of the preparation process of Fe_7Se_8@C. SEM images of (B) Fe_2O_3, (C) Fe_3O_4@C, and (D) Fe_7Se_8@C. (E) Cycling performance of Fe_7Se_8@C at 2.0 A g^{-1}[61]. Copyright 2022, Elsevier.

at 1 A g^{-1}, exhibiting negligible capacity decay over 1,000 cycles[63]. Wang *et al.* explored a carbon-coated Fe_7Se_8 nanosheet/nanorod composite (Fe_7Se_8@C/CNT-EG) through a one-step gas-phase pyrolysis method using expanded graphite (EG), selenium, and ferrocene as precursors[64]. The Fe_7Se_8@C/CNT-EG composite, featuring a 3D conductive network with abundant mesopores and a large surface area, exhibited enhanced Na^+ storage performance in an ester-based electrolyte. Notably, it demonstrated excellent cycling stability, retaining 97.5% of its capacity after 1,000 cycles at 1.0 A g^{-1}, and delivered a high rate capability of 325 mAh g^{-1} at 2.0 A g^{-1}[63]. Wang *et al.*, fabricated a hybrid material consisting of Fe_7Se_8 embedded in NC nanofibers (Fe_7Se_8 /N-CNFs) using a facile electrospinning technique[64]. As a SIB anode, the Fe_7Se_8/N-CNFs retained a high capacity of 286.3 mAh g^{-1} at an ultrahigh current density of 20 Ag^{-1}. The synergistic interaction between the Fe_7Se_8 nanoparticles and the cross-linked N-CNFs generated numerous defects and active Na^+ storage sites, shortened the Na^+ diffusion length, improved electrolyte infiltration, enhanced overall conductivity, and facilitated efficient electron/Na^+ transport, thereby promoting superior reaction kinetics[65].

Iron-based phosphides

Unlike iron oxides, which produce Na_2O (433 K, 5 × 10^{-8} S cm^{-1}) during Na^+ insertion and exhibit low conductivity, iron phosphates react with Na^+ to form Na_3P (room temperature, > 1 × 10^{-5} S cm^{-1}), thereby helping maintain electrochemical activity[66-70]. The Fe-P bond features unbound lone pairs of electrons in the 3p and 3d orbits, which significantly enhance the localized charge density, improving electronic conductivity[69-72]. Additionally, the Fe-P bond lengths, ranging from 2.186 to 2.447 Å, facilitate Na^+

migration within the FeP crystal structure, improving ionic conductivity and partially mitigating volumetric strain. The Na^+ storage process in FeP is as follows[66-70]:

$$FeP + xNa^+ + xe^- \leftrightarrow Na_xFeP \quad (17)$$

$$Na_xFeP + (3-x)Na^+ + (3-x)e^- \leftrightarrow Na_3P + Fe \quad (18)$$

However, challenges such as volume expansion during charging/discharging and limited electronic conductivity hinder large-scale application. Therefore, Yang *et al*. designed a FeP/graphite composite anode through a straightforward ball milling strategy[66]. This composite significantly enhanced conductivity and achieved a capacity of 134 mAh g^{-1} at 0.5 A g^{-1}[66]. To overcome Fe^0 agglomeration and poor conductivity in FeP, Xu *et al. in situ* encapsulated ultrafine FeP particles in porous carbon (FeP@C) via a MOF-derived phosphorization strategy [Figure 8A][67]. Energy-dispersive X-ray (EDX) elemental mapping signals [Figure 8B-E] indicate the co-existence of Fe, P, and C, with FeP particles fully wrapped in the carbon framework. As a Na^+ storage anode, the FeP@C electrode achieved capacities of 408, 366, 295, 235, 173, and 107 mAh g^{-1} at 0.1, 0.2, 0.5, 1.0, 2.0, and 4.0 A g^{-1}, respectively [Figure 8F]. Notably, it maintained 190 mAh g^{-1} over 500 cycles at 1.0 A g^{-1} [Figure 8G][67]. This outstanding cycling performance is attributed to the MOF-derived FeP@C, which suppresses Fe coarsening, improves conductivity, and buffers the volumetric strain. Li *et al.* further improved performance by encapsulating FeP nanodots within NC nanosheets to create an open-framework FeP@NC structure with high porosity and surface area[68]. Used as SIB anodes, FeP@NC delivered a capacity of 374 mAh g^{-1} over 2,000 cycles at 0.5 A g^{-1}[68]. This exceptional cycling stability is credited to the rationally designed hierarchical structure, which preserves integrity and promotes fast reaction kinetics. Wang *et al.* synthesized a hollow FeP@carbon structure wrapped in graphene (GR) (H-FeP@C@GR) via a hydrothermal method followed by carbon coating and phosphidation[69]. This anode retained a capacity of 400 mAh g^{-1} over 250 cycles at 0.1 A g^{-1}. The 3D hierarchical architecture endowed open pathways for electron/Na^+ transport and enhanced reaction kinetics. Moreover, the carbon shell facilitated the formation of a stable SEI layer, suppressing side reactions[69]. Jiang *et al.* fabricated FeP nanoparticles embedded in N,P-doped carbon frameworks (FeP@PNC) using a phytic acid-derived self-assembly process[70]. This anode holds a high reversible capacity of 340.1 mA h g^{-1} at 0.1 A g^{-1} and remarkable cycling capability, maintaining 224.5 mA h g^{-1} at 0.5 A g^{-1} over 4,500 cycles. These superior electrochemical properties stem from the unique 3D heterostructure, which enhances structural stability, accelerates reaction kinetics, and prevents nanoparticle aggregation during sodiation/desodiation.

Compared to conventional power-based anodes, self-supported electrodes are typically grown on a conductive metal/carbon matrix, which can mitigate the side effects of binders and enhance the energy density of SIBs. Furthermore, such binder-free electrodes are intrinsically flexible, ultrathin, lightweight, and bendable, allowing them to maximize space utilization in electronic devices. For instance, Shi *et al*. reported a free-standing FeP@NPC film anode for SIBs, where FeP nanoparticles were embedded in a 3D cross-linked N,P-doped carbon (NPC) fiber network[71]. The FeP nanoparticles were *in situ* confined within the N,P-doped carbon fibers via thermal treatment of PAN nanofibers. The 3D-connected NPC framework offered efficient electron/ion transport pathways and featured void spaces to accommodate volumetric strain during Na^+ extraction/insertion. This FeP@NPC anode achieved a capacity of 557 mAh g^{-1} at 0.1 A g^{-1} over 1,000 cycles. Their work broadens the approach to fabricating binder-free phosphide anodes for flexible SIBs[71]. Similarly, Park *et al*. developed a self-supported film composed of superfine FeP@C particles dispersed on P-doped graphene (FeP@C@PG) through solvent-free pyrogenic decomposition followed by roll pressing[72]. PA served as both the phosphorus and carbon source, enabling *in-situ* confinement of

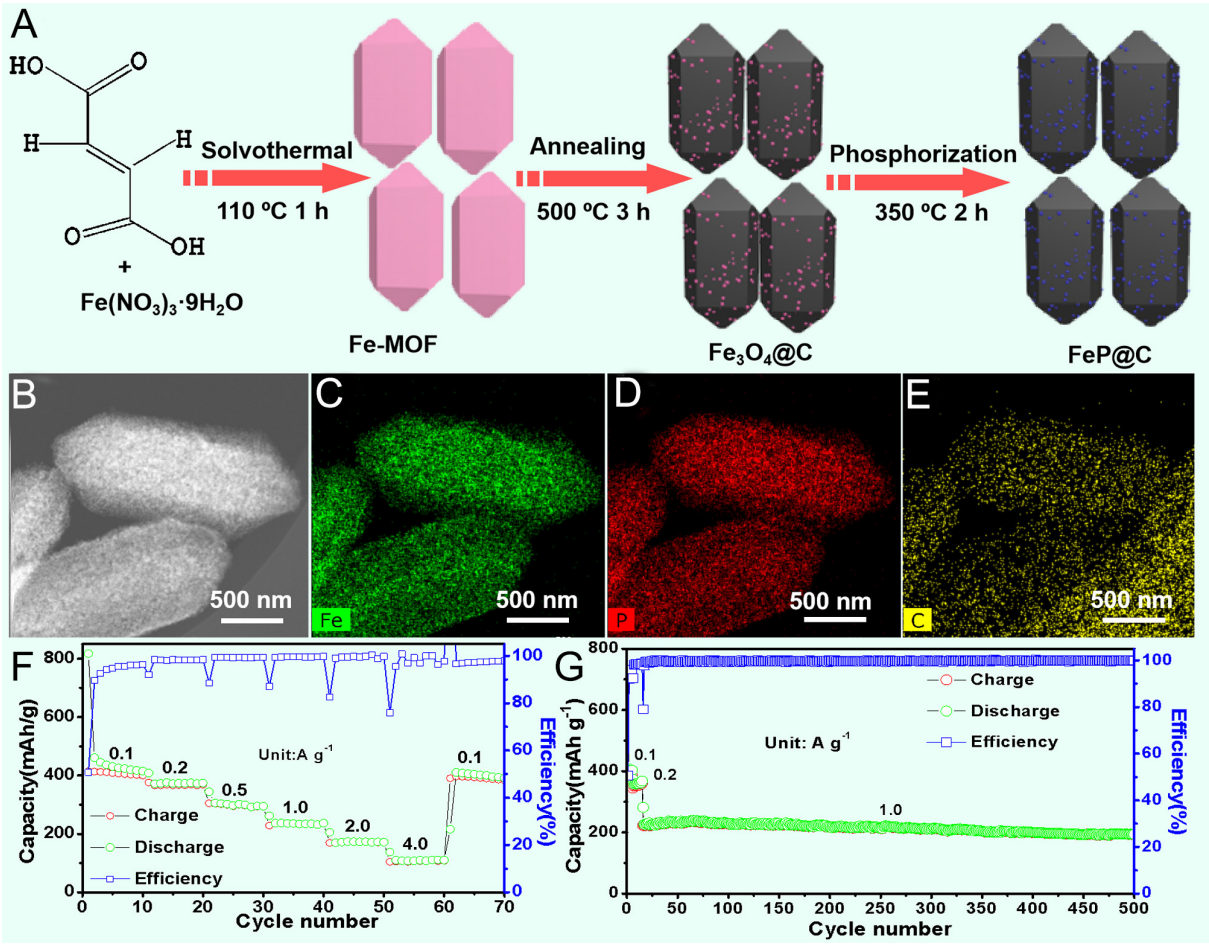

Figure 8. (A) Schematic illustration of the preparation process of FeP@C. (B) Dark-field TEM image; (C-E) corresponding EDX mapping signals of Fe (C), P (D), and C (E) elements. (F) Rate performance of FeP@C measured from 0.1 to 4.0 A g^{-1} and (G) cycling performance of FeP@C at 2.0 A g^{-1} [67]. Copyright 2019, Elsevier.

ultrafine FeP particles within the P-doped carbon matrix. This hierarchical structure accelerated diffusion kinetics, mitigated significant changes, and suppressed the aggregation/pulverization of FeP particles during charging/discharging. As a result, the FeP@C@PG film exhibited a capacity of 536.6 mAh g^{-1} over 1,000 cycles at 1 A g^{-1}, and a high rate capability of 440.7 mAh g^{-1} at 5 A g^{-1}.

Compared with other oxides and sulfides, iron-based phosphide materials have a lower charging/discharging potential, making them more suitable as SIB anodes. If their electrochemical properties can be further improved, they hold great promise for future applications.

Iron-based fluorides

Iron-based fluorides can support multi-electron transfer through multi-step electrochemical reactions, enabling them to reach high specific capacities[73-77]. Common iron-based fluorides include FeF_2, FeF_3, and hydrated forms. For instance, FeF_3 exhibits an ultrahigh theoretical capacity of 712 mAh g^{-1} along with a relatively high operating voltage, which attracted considerable attention for its potential as a cathode material in SIBs[77-82]. The Na^+ storage mechanism of FeF_3 is as follows[77-82]:

$$FeF_3 + xNa^+ + xe^- \leftrightarrow Na_xFeF_3 \quad (19)$$

$$FeF_3 + (3\text{-}x)Na^+ + (3\text{-}x)e^- \leftrightarrow 3NaF + Fe \quad (20)$$

At present, the electrochemical performance of fluoride materials remains unsatisfactory due to significant voltage hysteresis and sluggish reaction kinetics, resulting in rapid capacity decay[74,80-82]. Therefore, developing iron-based fluoride cathodes for SIBs and enhancing their electrochemical properties is of great importance.

One major challenge is the severe pulverization of iron fluorides during cycling, which results in rapid structural degradation and capacity fading. To address this, Zhang *et al.* designed an amorphous FeF_3/C nanocomposite cathode using Fe-MOF nanorods as precursors via high-temperature carbonization and fluorination[74]. This FeF_3/C cathode demonstrated excellent cycling stability, retaining 126.7 mAh g^{-1} over 100 cycles at 75 mA g^{-1}[74]. The improved performance is ascribed to the amorphous structure and the porous carbon backbone formed from the carbonized organic ligands of the Fe-MOF, which facilitate Na^+/electron diffusion and enhance reaction kinetics. Sun *et al.* developed a free-standing FeF_3 cathode and employed sodium-difluoro(oxalate)borate (NaDFOB) as the electrolyte salt for SIBs [Figure 9A][75]. XRD analysis [Figure 9B] confirmed that the synthesized material matched the hexagonal FeF_3 phase. SEM images [Figure 9C and D] reveal that FeF_3 nanoparticles were uniformly distributed within or on the surface of the NFs. TEM images [Figure 9E] further show that FeF_3 crystals are well- encapsulated within the carbon matrix. As shown in Figure 9F, cells using NaDFOB demonstrated superior cycling stability compared to those using $NaPF_6$ or $NaClO_4$ over 120 cycles. Moreover, as illustrated in Figure 9G, cells using a DEC/EC/DMC solvent mixture achieved the highest capacity retention of 69.4%, significantly outperforming those using EC/DEC (28.17%) or EC/DMC (31.4%). This enhanced performance is associated with the synergistic effect between the nanoconfined FeF_3 cathode and the NaDFOB electrolyte. Quantum mechanical calculations revealed that $DFOB^-$ facilitated the formation of a thin CEI layer on the FeF_3-CNFs, improving stability[75]. Despite these advancements, the practical application of FeF_3-based cathodes remains hindered by low capacity utilization and poor cycling performance. Sun *et al.* investigated various ionic liquid (IL) electrolytes to enhance the Na^+ storage performance of FeF_3 across a wide temperature range[76]. They found that the $Pyr_{1,4}FSI$ electrolyte exhibited an ignorable decay rate of ~0.023% per cycle over 1,000 cycles. $Pyr_{1,3}FSI$ showed better stability at elevated temperatures. A protective and ion-conductive CEI film was formed during cycling in ILs, suppressing side reactions, especially at high temperatures[76].

Ma *et al.* proposed a FeF_3-Fe-RGO composite as a cathode for SIBs, in which a conductive matrix of metallic Fe and RGO was formed *in situ* from a single FeF_2 grain during electrochemical cycling[77]. This FeF_3-Fe-RGO cathode delivered a capacity of 150 mAh g^{-1} at 0.05 A g^{-1} and maintained a specific capacity of 60 mAh g^{-1} even at 2.0 A g^{-1}[77]. The superior electrochemical performance is attributed to the enhanced electronic conductivity provided by the RGO and metallic Fe-based conductive framework. This design strategy could be extended to other electrode materials that offer high capacity but suffer from low electrical conductivity.

FeF_2 has also emerged as a promising conversion-type cathode material for SIBs. Accordingly, Maulana *et al.* synthesized FeF_2 nanoparticles encapsulated in N-doped graphitic carbon (FeF_2@NGC) for use as a SIB cathode[78]. The optimized FeF_2@NGC delivered a high reversible capacity of 214.2 mAh g^{-1} over 500 cycles at 300 mA g^{-1}, with a low capacity fading rate of just 0.042% per cycle, indicating excellent long-term stability[78]. Similarly, Ni *et al.* prepared FeF_2@mesoporous hollow carbon spheres (FeF_2@MHCS) as cathodes for SIBs[79]. The hierarchical structure of FeF_2@MHCS suppressed agglomeration, facilitated Na^+/

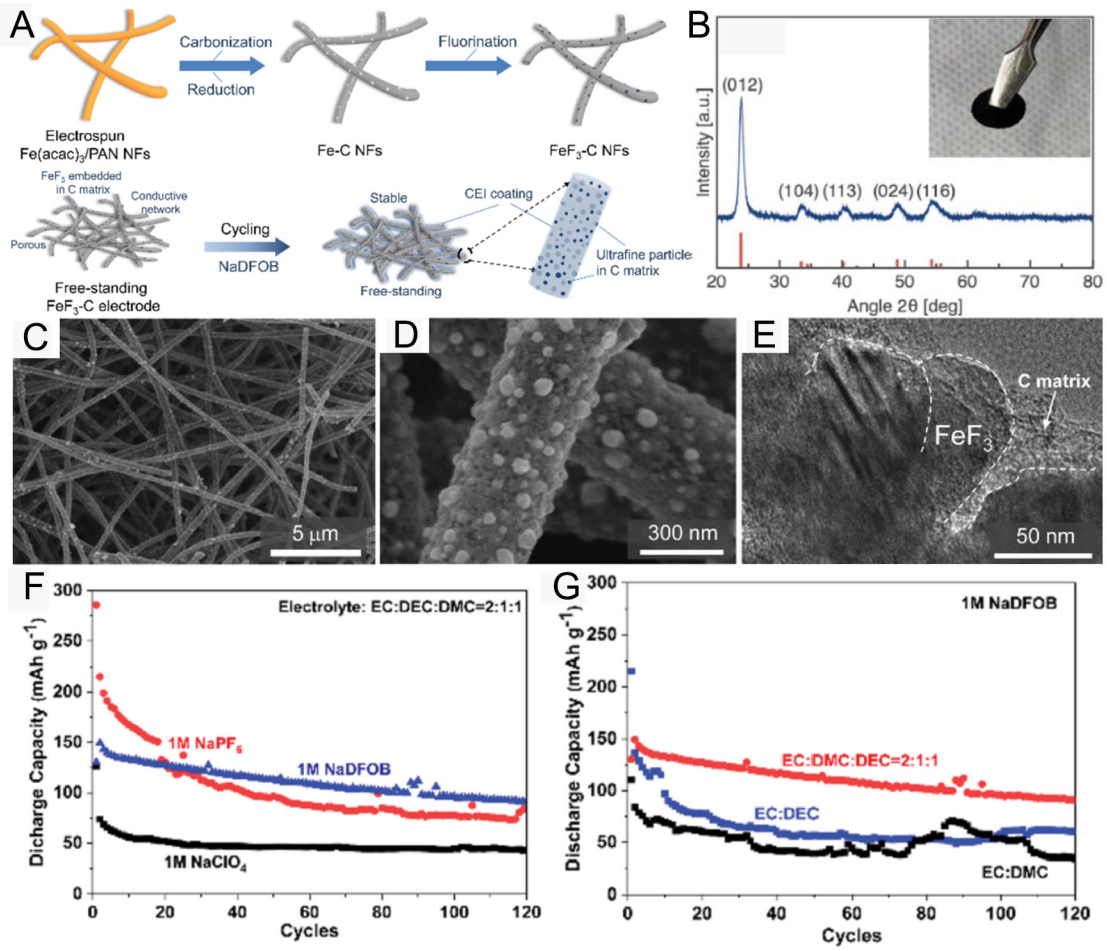

Figure 9. (A) Schematic of the preparation procedures of FeF_3-C NFs and FeF_3-C electrode cycled in the NaDFOB electrolyte; (B) XRD pattern of FeF_3-C NFs cathode; (C and D) SEM images of FeF_3-CNFs; (E) High-resolution TEM image of FeF_3-CNFs. (F) Cycling performance of FeF_3-CNFs with different sodium salts and (G) cycling performance of FeF_3-CNFs in 1M NaDFOB electrolyte with different solvents[75]. Copyright 2020, Royal Society of Chemistry.

electron diffusion, and mitigated the volume variation during cycling. This cathode achieved a capacity of 220 mAh g^{-1} at 0.03 A g^{-1} and 64 mA h g^{-1} at 10 A g^{-1}, and retained 112 mA h g^{-1} over 100 cycles at 0.2 A g^{-1}[79]. In another study, Ni *et al.* fabricated a FeF_2-RGO nanocomposite cathode using poly(acrylic acid) (PAA) as a binder for SIBs[80]. The use of PAA was found to stabilize the electrode structure, improve the utilization of active materials, and significantly enhance Na^+ storage performance. The FeF_2-RGO cathode achieved superior cycling stability (175 mAh g^{-1} at 0.2 A g^{-1}) and good rate capability (78 mAh g^{-1} at 10 A g^{-1})[80].

Despite these advancements, the poor electronic conductivity and side reactions of FeF_3 cathodes result in sluggish reaction kinetics and rapid capacity decay during cycling, impeding their large-scale application. To address this, Liu *et al.* employed a surface modification method, synthesizing hollow $FeF_3{\cdot}0.33H_2O$ microspheres through a solvothermal approach followed by coating with $AlPO_4$[81]. This surface treatment significantly reduced charge-transfer resistance and improved Na^+ diffusion. Compared to pristine $FeF_3{\cdot}0.33H_2O$, the $AlPO_4$-coated version (with 4 wt.% $AlPO_4$) displayed an initial capacity of 290 mAh g^{-1} and retained 211 mAh g^{-1} over 80 cycles within a voltage window of 1.2~4.0 V[79]. The enhanced electrochemical properties were ascribed to the hierarchical porous structure that promotes electrolyte permeation and rapid Na^+/electron transport. Moreover, the multifunctional $AlPO_4$ coating enhanced

overall conductivity, reduced volumetric strain, and suppressed surface side reactions during cycling.

In summary, coupling iron-based fluoride nanoparticles with conductive carbon materials can effectively improve electrical conductivity, alleviate volume expansion and particle agglomeration, and enhance the overall electrochemical properties of SIB cathodes.

Other iron-based materials

Other iron-based materials - such as $FeTiO_3$, $FeTe_2$, $FePS_3$, $FePO_4$, and $Fe_2(SO_4)_3$ - have also shown promise for application in SIBs due to their relatively high theoretical specific capacities[82-87]. Researchers have explored strategies to control the growth and microstructure of these materials to improve their cycling stability and rate performance. For example, two-dimensional (2D) $FePS_3$ nanosheets, a typical ternary metal phosphosulfide, were synthesized via ultrasonic exfoliation. A $FePS_3$ nanosheets@MXene composite was subsequently fabricated by *in situ* mixing of the exfoliated nanosheets with ultrathin MXene layers[83]. This hybrid material improved electronic conductivity and increased the specific surface area, thus accelerating Na^+ diffusion and alleviating volumetric strain during repeated cycling. As a result, the $FePS_3$ nanosheets@MXene composite reached a reversible capacity of 676.1 mAh g^{-1} over 90 cycles at 0.1 A g^{-1}[83]. This work provides a valuable pathway for the development of 2D/2D conversion-type electrode materials with enhanced performance for SIBs. In addition, tellurium-based materials have attracted attention due to tellurium's inherently high electrical conductivity. Iron tellurides, in particular, have been investigated for Na^+ storage applications. Recently, $FeTe_2$ nanoparticles embedded in nitrogen-doped carbon nanofibers ($FeTe_2$/CNFs) were synthesized via electrospinning[84]. The $FeTe_2$/CNF anode demonstrated an initial capacity of 406.8 mAh g^{-1} and retained 221.3 mAh g^{-1} over 1,000 cycles at 1 A g^{-1}. These outstanding electrochemical properties are attributed to the synergistic interaction between the $FeTe_2$ particles and the carbon nanofiber matrix, which buffers volume changes and enhances structural stability during cycling[84]. $FePO_4$, with a high theoretical capacity of 175 mAh g^{-1}, can be easily synthesized on a large scale through a facile precipitation procedure at room temperature, making it a promising cathode candidate for SIBs[88]. Furthermore, monoclinic $Fe_2(SO_4)_3$, when coupled with a Na anode, exhibits an average operating voltage of ~3.25 V and can store 1.8 Na^+, delivering a specific capacity of ~120 mAh g^{-1}, thus emerging as another potential cathode material[89].

Iron-based materials offer several advantages, including abundant raw resources and low production costs. A wide variety of iron-containing compounds and metal composites have been explored as electrode materials, leading to significant advancements in the development of both cathode and anode materials for SIBs.

SUMMARY AND OUTLOOK

This review summarizes recent advances in the design of tailored nanostructures and the development of straightforward methods to enhance the electrochemical properties of conversion-type iron-based electrodes. While numerous modification approaches have been employed to improve the long-cycling stability of these electrodes, conventional techniques still present certain limitations. As shown in Table 1, nanostructure engineering effectively enhances both the cycling stability and rate performance of iron-based materials. Additionally, novel MOF-derived methods have been applied in the synthesis of iron-based materials. During subsequent processing, organic functional groups form *in situ* coatings on the iron-based nanounits, which markedly enhance their cycling and rate capabilities.

From an application standpoint, the initial Coulomb efficiency and overall electrochemical performance of certain iron-based electrodes still require significant improvement and further investigation. It is essential to

Table 1. Comparison of the electrochemical properties of conversion-type iron-based materials for SIBs

Type	Electrode materials	Current density ($mA\ g^{-1}$)	Specific capacity ($mA\ h\ g^{-1}$)	Cycle number (cycles)	Voltage region (V)	Reference
Iron-based oxides	Fe_2O_3@MIL-101(Fe)/C	200	662	200	0.01-3.0	[18]
	MFe_2O_3@N-HCNs	2,000	363	4,500	0.01-3.0	[20]
	Fe_2O_3/rGO	50	~500	100	0.01-3.0	[22]
	Fe_2O_3-C@CF	30	530	100	0.01-3.0	[23]
	Fe_2O_3 nanorods	50	252	100	0.01-3.0	[24]
	a-Fe_2O_3/pBC-N	100	408	350	0.01-3.0	[25]
	3D-0D graphene-Fe_3O_4	50	312	200	0.01-3.0	[26]
	Fe_3O_4@C@G	100	180	600	0.01-3.0	[27]
	Fe_3O_4@C@PPy	1,000	640	100	0.01-2.5	[28]
	Fe_3O_4 QD@C-GN	2,000	343	1,000	0.01-3.0	[29]
	Fe_3O_4/C/P	200	1,390	200	0.01-3.0	[30]
	Fe_3O_4-CNFs	500	358.1	200	0.01-3.0	[31]
Iron-based sulfides	FeS_2	200	94	100	0.01-3.0	[33]
	Mesoporous FeS_2	1,000	711.1	450	0.01-2.8	[34]
	FeS_2-CGS	1,000	855.9	200	0.01-3.0	[35]
	CHS-FeS_2	500	546.5	100	0.01-2.8	[36]
	FeS_2@CF-NS	5,000	431.1	700	0.01-3.0	[37]
	$Co_{0.5}Fe_{0.5}S_2$	2,000	220	5,000	0.8-2.9	[38]
	FeS_2@C	100	616	100	0.5-3.0	[39]
	FeS_2@C yolk-shell	100	511	100	0.1-2.0	[40]
	Pitaya-Structured FeS_2@C	600	415	120	0.5-2.5	[41]
	FeS_2@G@CNF	3,000	305.5	2,450	0.5-2.5	[42]
	Porous FeS nanofibers	500	592	150	0.01-3.0	[43]
	FeS/C	10,000	300.4	10,000	0.01-3.0	[44]
	FeS/NC	1,000	326	500	0.01-3.0	[45]
	Mn-doped FeS/NC	8,000	206.2	8,000	0.4-2.8	[46]
	3D porous FeS@NC	1,500	254	1,110	0.5-3	[47]
Iron-based selenides	$FeSe_2$ clusters	1,000	515	400	0.5-2.9	[50]
	Hierarchical porous $FeSe_2$	10,000	333	1,800	0.01-3.0	[51]
	$FeSe_2$-AC	500	379	150	0.01-3.0	[52]
	$FeSe_2$/GNS-400	25,000	227	800	0.01-2.8	[53]
	$FeSe_2$@C Microrods	5,000	401.3	2,000	0.5-2.8	[54]
	$FeSe_2$@NC	5,000	372.9	1,000	0.01-3.0	[55]
	P-$FeSe_2$/NCF	2,000	507	200	0.01-3.0	[56]
	CNT/$FeSe_2$/C	100	546	100	0.01-3.0	[57]
	Fe_7Se_8 NRBs	200	294	1,800	0.4-2.8	[58]
	Fe_7Se_8@C@$MoSe_2$	1,000	345	600	0.01-3.0	[60]
	Fe_7Se_8@C nanotubes	2,000	319	720	0.5-3.0	[61]
	Fe_7Se_8@NC	5,000	185.6	6,000	0.5-3.0	[62]
	Fe_7Se_8@C/N nanoboxes	5,000	316	1,000	0.5-2.5	[63]
	Fe_7Se_8@C/CNT-EG	1,000	336	1,000	0.01-3.0	[64]
Iron-based phosphides	FeP/graphite	50	240	70	0.01-1.5	[66]
	MOF-derived FeP@C	100	387	100	0.01-3.0	[67]
	FeP@NC	500	375	2,000	0.01-3.0	[68]
	H-FeP@C@GR	100	400	250	0.01-3.0	[69]
	FeP@PNC	500	224.5	4,500	0.01-3.0	[70]
	FeP@NPC film	1,000	253	300	0.01-3.0	[71]
	FeP@C@PG film	1,000	536.6	1,000	0.01-3.0	[72]

FeF_3/CNF	20	~161	100	1.2-4.2	[75]
FeF_3/Fe/RGO	100	70	1,000	0.8-4.5 V	[77]
FeF_2	300	214.2	500	1.2-4.2	[78]
FeF_2@MHCS	200	112	100	1.5-4.5	[79]
FeF_2-rGO	200	85	200	1.5-4.5	[80]
$FeF_3{\cdot}0.33H_2O/AlPO_4$	200	211	80	1.2-4.0	[81]

explore in greater depth the relationship between crystal structure, electronic structure, and sodium storage performance. Through rational element doping and precise crystal structure engineering, the conversion reaction mechanisms of iron-based materials can be optimized, increasing the number of active sites involved in the reaction and thereby enhancing the specific capacity. To further improve the cycling stability of iron-based electrodes, several strategies can be employed. On the one hand, nanostructure design - such as the fabrication of nanoparticles, nanowires, and nanotubes - can shorten the Na^+ diffusion paths and alleviate the volume changes during charging/discharging. On the other hand, surface coating and composite fabrication techniques are also effective. For example, coating iron-based materials with conductive carbon or other stable compounds can not only enhance electronic conductivity but also suppress side reactions between the active material and the electrolyte, thereby strengthening structural stability. Optimizing the electronic conductivity and Na^+ diffusion rate is crucial to improving the rate capability of these materials. This can be achieved by incorporating highly conductive additives or constructing three-dimensional conductive networks to facilitate electron transfer. Additionally, designing materials with large transport channels or introducing structural defects can accelerate Na^+ ion diffusion. Previous studies have also shown that some iron-based materials can help stabilize the SEI[90,91]. Thus, iron-based electrodes can be combined with other electrode materials to further enhance overall electrochemical performance. With ongoing technological advances and breakthroughs in synthesis techniques, the advantages of iron-based materials are expected to become increasingly evident.

For future development, attention should also be given to exploring functional electrolytes and additives that are compatible with the wide-temperature operational requirements of iron-based electrodes. Moreover, iron-based electrodes have been investigated for LIBs[92,93], indicating the potential for iron-based cathodes such as FeF_3, FeF_2, and $Fe_2(SO_4)_3$ to be paired with solid-state electrolytes in solid-state sodium metal batteries, thereby further improving energy density.

Advanced characterization techniques are essential for probing the structural and interfacial stability of iron-based materials. In particular, *in situ* techniques such as XRD, TEM, and XPS enable real-time monitoring of structural and interfacial evolution during sodiation/desodiation. ToF-SIMS can offer detailed compositional analysis of the SEI through depth profiling. Nevertheless, the lack of a clear mechanistic understanding still hinders the widespread practical application of these materials. In conclusion, structural optimization, when combined with targeted surface engineering, can significantly improve the electrochemical properties of iron-based electrodes. It is hoped that this review will shed light on the rational design of conversion-type electrodes for SIBs.

DECLARATIONS

Authors' contributions

Writing of the original draft: Chen, S.; Ye, S.
Review & editing: Xu, X.; Sun, H.
Conceptualization, review, and supervision: Fan, W.; Zhao, J.; Huo, Y.

Availability of data and materials
Not applicable.

Financial support and sponsorship
This work was supported by the National Natural Science Foundation of China (No. 52301266), Guangdong Basic and Applied Basic Research Foundation (No. 2025A1515012152), the Science and Technology Planning Project of Guangzhou (No. 2024A04J3332), and the Chenzhou National Sustainable Development Agenda Innovation Demonstration Zone Provincial Special Project (No. 2023sfq11).

Conflicts of interest
Fan, W. and Zhao, J. are affiliated with Guangzhou Tinci Materials Technology Co., Ltd., while the other authors have declared that they have no conflicts of interest.

Ethical approval and consent to participate
Not applicable.

Consent for publication
Not applicable.

REFERENCES
1. Wu, F.; Maier, J.; Yu, Y. Guidelines and trends for next-generation rechargeable lithium and lithium-ion batteries. *Chem. Soc. Rev.* **2020**, *49*, 1569-614. DOI PubMed
2. Sun, Y.; Li, Y.; Gong, Y.; et al. Constructing three-dimensional architectures to design advanced anodes materials for sodium-ion batteries: from nanoscale to microscale. *Energy. Mater.* **2024**, *4*, 400002. DOI
3. Liu, Z.; Song, Y.; Fu, S.; et al. Multiphase manganese-based layered oxide for sodium-ion batteries: structural change and phase transition. *Microstructures* **2024**, *4*, 2024036. DOI
4. Huang, Y.; Zeng, W.; Li, K.; Zhu, X. Na-deficient P2-type layered oxide cathodes for practical sodium-ion batteries. *Microstructures* **2024**, *4*, 2024027. DOI
5. Zhang, R.; Chen, H.; Yue, H. Room-temperature synthesis of layered open framework cathode for sodium-ion batteries. *Chin. Chem. Lett.* **2023**, *34*, 107580. DOI
6. Yin, H.; Han, D.; Wang, W.; et al. Bimetallic sulfide anodes based on heterojunction structures for high-performance sodium-ion battery anodes. *Chin. Chem. Lett.* **2024**, 110537. DOI
7. Li, X.; Liu, X.; Xiang, Y.; Zheng, Q.; Wei, X.; Lin, D. Metal-organic frameworks derived carbon-coated ZnSe/$Co_{0.85}$Se@N-doped carbon microcuboid as an advanced anode material for sodium-ion batteries. *Chin. Chem. Lett.* **2022**, *33*, 3197-202. DOI
8. Wan, Y.; Liu, Y.; Chao, D.; Li, W.; Zhao, D. Recent advances in hard carbon anodes with high initial Coulombic efficiency for sodium-ion batteries. *Nano. Mater. Sci.* **2023**, *5*, 189-201. DOI
9. Rehman, A.; Saleem, S.; Ali, S.; Abbas, S. M.; Choi, M.; Choi, W. Recent advances in alloying anode materials for sodium-ion batteries: material design and prospects. *Energy. Mater.* **2024**, *4*, 400068. DOI
10. Wang, Y.; Kuang, Y.; Cui, J.; et al. Self-template construction of hierarchical Bi@C microspheres as competitive wide temperature-operating anodes for superior sodium-ion batteries. *Nano. Lett.* **2024**, *24*, 15242-51. DOI
11. Zhao, J.; Zhang, S.; Liu, W.; Du, Z.; Fang, H. Fe_3O_4/PPy composite nanospheres as anode for lithium-ion batteries with superior cycling performance. *Electrochim. Acta.* **2014**, *121*, 428-33. DOI
12. Zhao, Y.; Wang, F.; Wang, C.; et al. Encapsulating highly crystallized mesoporous Fe_3O_4 in hollow N-doped carbon nanospheres for high-capacity long-life sodium-ion batteries. *Nano. Energy.* **2019**, *56*, 426-33. DOI
13. Wei, C.; Wang, R.; Wu, Z.; et al. Revealing the size effect of FeS_2 on solid-state battery performances at different operating temperatures. *Chin. Chem. Lett.* **2024**, *35*, 108717. DOI
14. Qiu, D.; Gao, A.; Zhao, W.; et al. Fast-charging degradation mechanism of two-dimensional FeSe anode in sodium-ion batteries. *ACS. Energy. Lett.* **2023**, *8*, 4052-60. DOI
15. Hou, B. H.; Wang, Y. Y.; Ning, Q. L.; et al. An FeP@C nanoarray vertically grown on graphene nanosheets: an ultrastable Li-ion battery anode with pseudocapacitance-boosted electrochemical kinetics. *Nanoscale* **2019**, *11*, 1304-12. DOI
16. Wu, F.; Srot, V.; Chen, S.; et al. 3D honeycomb architecture enables a high-rate and long-life iron (III) fluoride-lithium battery. *Adv.*

Mater. **2019**, *31*, e1905146. DOI

17. Philippe, B.; Valvo, M.; Lindgren, F.; Rensmo, H.; Edström, K. Investigation of the electrode/electrolyte interface of Fe_2O_3 composite electrodes: Li vs Na batteries. *Chem. Mater.* **2014**, *26*, 5028-41. DOI
18. Li, C.; Hu, Q.; Li, Y.; et al. Hierarchical hollow Fe_2O_3@MIL-101(Fe)/C derived from metal-organic frameworks for superior sodium storage. *Sci. Rep.* **2016**, *6*, 25556. DOI PubMed PMC
19. Li, L.; Li, H.; Liu, L.; Yan, X.; Long, Y.; Han, W. Amorphous Fe_2O_3 anchored on N-doped graphene with internal micro-channels as an active and durable anode for sodium-ion batteries. *Nanomaterials* **2024**, *14*, 937. DOI PubMed PMC
20. Chen, M.; Niu, D.; Mao, J.; et al. A movable Fe_2O_3 core in connected hierarchical pores for ultrafast intercalation/deintercalation in sodium-ion batteries. *ACS. Appl. Energy. Mater.* **2021**, *4*, 5888-96. DOI
21. Li, D.; Zhou, J.; Chen, X.; et al. Amorphous Fe_2O_3/graphene composite nanosheets with enhanced electrochemical performance for sodium-ion battery. *ACS. Appl. Mater. Interfaces.* **2016**, *8*, 30899-907. DOI
22. Li, T.; Qin, A.; Yang, L.; et al. In situ grown Fe_2O_3 single crystallites on reduced graphene oxide nanosheets as high performance conversion anode for sodium-ion batteries. *ACS. Appl. Mater. Interfaces.* **2017**, *9*, 19900-7. DOI
23. Bhar, M.; Ghosh, S.; Martha, S. K. Designing freestanding electrodes with Fe_2O_3-based conversion type anode material for sodium-ion batteries. *J. Alloys. Compd.* **2023**, *948*, 169670. DOI
24. Zhao, D.; Xie, D.; Liu, H.; Hu, F.; Wu, X. Flexible α-Fe_2O_3 nanorod electrode materials for sodium-ion batteries with excellent cycle performance. *Funct. Mater. Lett.* **2018**, *11*, 1840002. DOI
25. Shi, L.; Li, Y.; Zeng, F.; et al. In situ growth of amorphous Fe_2O_3 on 3D interconnected nitrogen-doped carbon nanofibers as high-performance anode materials for sodium-ion batteries. *Chem. Eng. J.* **2019**, *356*, 107-16. DOI
26. Liu, H.; Jia, M.; Zhu, Q.; et al. 3D-0D graphene-Fe_3O_4 quantum dot hybrids as high-performance anode materials for sodium-ion batteries. *ACS. Appl. Mater. Interfaces.* **2016**, *8*, 26878-85. DOI
27. Tao, X.; Li, Y.; Wang, H. G.; et al. Multi-heteroatom-doped dual carbon-confined Fe_3O_4 nanospheres as high-capacity and long-life anode materials for lithium/sodium ion batteries. *J. Colloid. Interface. Sci.* **2020**, *565*, 494-502. DOI
28. Biswal, R.; Shukla, V.; Janakiraman, S.; Ghosh, S.; Adyam, V. Novel dual core@shell Fe_3O_4@C@polypyrrole (PPy) composite for sodium ion batteries. *Mater. Today. Proc.* **2020**, *33*, 5088-92. DOI
29. Qi, L. Y.; Zhang, Y. W.; Zuo, Z. C.; et al. *In situ* quantization of ferroferric oxide embedded in 3D microcarbon for ultrahigh performance sodium-ion batteries. *J. Mater. Chem. A.* **2016**, *4*, 8822-9. DOI
30. Qin, G.; Duan, J.; Yang, Y.; Liu, F. Magnetic field facilitated resilient chain-like Fe_3O_4/C/red P with superior sodium storage performance. *ACS. Appl. Mater. Interfaces.* **2018**, *10*, 6441-52. DOI
31. Huang, Y.; Zhou, J.; Zhang, Y.; et al. Encapsulating hollow Fe_3O_4 in intertwined N-doped carbon nanofibers for high-performance supercapacitors and sodium-ion batteries. *J. Alloys. Compd.* **2022**, *918*, 165672. DOI
32. Kitajou, A.; Yamaguchi, J.; Hara, S.; Okada, S. Discharge/charge reaction mechanism of a pyrite-type FeS_2 cathode for sodium secondary batteries. *J. Power. Sources.* **2014**, *247*, 391-5. DOI
33. Li, Z.; Zhang, Y.; Li, X.; et al. Reacquainting the electrochemical conversion mechanism of FeS_2 sodium-ion batteries by operando magnetometry. *J. Am. Chem. Soc.* **2021**, *143*, 12800-8. DOI
34. Zhang, Z.; Zhong, X.; Zhang, Y.; et al. Scalable synthesis of mesoporous FeS_2 nanorods as high-performance anode materials for sodium-ion batteries. *Rare. Met.* **2022**, *41*, 21-8. DOI
35. Kandula, S.; Youn, B. S.; Cho, J.; Lim, H.; Gon Son, J. FeS_2@N-C nanorattles encapsulated in N/S dual-doped graphene/carbon nanotube network composites for high performance and high rate capability anodes of sodium-ion batteries. *Chem. Eng. J.* **2022**, *439*, 135678. DOI
36. Ma, L.; Hou, B.; Zhang, H.; et al. Regulation of MIL-88B(Fe) to design FeS_2 core-shelled hollow sphere as high-rate anode for a full sodium-ion battery. *Chem. Eng. J.* **2023**, *453*, 139735. DOI
37. Lu, Z.; Zhai, Y.; Wang, N.; et al. FeS_2 nanoparticles embedded in N/S co-doped porous carbon fibers as anode for sodium-ion batteries. *Chem. Eng. J.* **2020**, *380*, 122455. DOI
38. Zhang, K.; Park, M.; Zhou, L.; et al. Cobalt-doped FeS_2 nanospheres with complete solid solubility as a high-performance anode material for sodium-ion batteries. *Angew. Chem. Int. Ed.* **2016**, *55*, 12822-6. DOI
39. Man, Z.; Li, P.; Zhou, D.; et al. Two birds with one stone: FeS_2@C yolk-shell composite for high-performance sodium-ion energy storage and electromagnetic wave absorption. *Nano. Lett.* **2020**, *20*, 3769-77. DOI
40. Liu, Z.; Lu, T.; Song, T.; Yu, X.; Lou, X. W.; Paik, U. Structure-designed synthesis of FeS_2@C yolk-shell nanoboxes as a high-performance anode for sodium-ion batteries. *Energy. Environ. Sci.* **2017**, *10*, 1576-80. DOI
41. Xu, X.; Liu, J.; Liu, Z.; et al. Robust pitaya-structured pyrite as high energy density cathode for high-rate lithium batteries. *ACS. Nano.* **2017**, *11*, 9033-40. DOI
42. Chen, C.; Yang, Y.; Tang, X.; et al. Graphene-encapsulated FeS_2 in carbon fibers as high reversible anodes for Na^+/K^+ batteries in a wide temperature range. *Small* **2019**, *15*, e1804740. DOI
43. Cho, J. S.; Park, J.; Kang, Y. C. Porous FeS nanofibers with numerous nanovoids obtained by Kirkendall diffusion effect for use as anode materials for sodium-ion batteries. *Nano. Res.* **2017**, *10*, 897-907. DOI
44. Han, M.; Liu, J.; Deng, C.; et al. Yolk-shell structure and spin-polarized surface capacitance enable FeS stable and fast ion transport in sodium-ion batteries. *Adv. Energy. Mater.* **2024**, *14*, 2400246. DOI
45. Liu, Y.; Zhong, W.; Yang, C.; et al. Direct synthesis of FeS/N-doped carbon composite for high-performance sodium-ion batteries. *J.*

Mater. Chem. A. **2018**, *6*, 24702-8. DOI

46. Chen, H.; Yang, X.; Lv, P.; Tian, P.; Wan, S.; Liu, Q. Mn-doped FeS with larger lattice spacing as advance anode for sodium ion half/full battery. *Chem. Eng. J.* **2022**, *450*, 137960. DOI
47. Yuan, J.; Mu, M.; Xu, X.; et al. Three-dimensional porous FeS@N doped carbon nanosheets for high-rate and high-stable sodium/potassium storage. *Compos. Part. B. Eng.* **2022**, *247*, 110300. DOI
48. Zhang, J.; Meng, Z.; Yang, D.; et al. Enhanced interfacial compatibility of FeS@N,S-C anode with ester-based electrolyte enables stable sodium-ion full cells. *J. Energy. Chem.* **2022**, *68*, 27-34. DOI
49. Huang, X.; He, Q.; Xun, J.; et al. Constructing strain-alleviated structures in ultrathin FeS/C composites for durable lithium and sodium storage. *Sci. China. Mater.* **2023**, *66*, 2601-12. DOI
50. Wei, X.; Tang, C.; An, Q.; et al. $FeSe_2$ clusters with excellent cyclability and rate capability for sodium-ion batteries. *Nano. Res.* **2017**, *10*, 3202-11. DOI
51. Wang, L.; Bai, K.; Lu, Y.; Mo, W.; Zhang, L. Controllable hierarchical porous $FeSe_2$ with excellent long cycle lifespan as anode materials for sodium-ion battery. *J. Power. Sources.* **2024**, *592*, 233913. DOI
52. Park, G. D.; Kim, J. H.; Kang, Y. C. Large-scale production of spherical $FeSe_2$-amorphous carbon composite powders as anode materials for sodium-ion batteries. *Mater. Charact.* **2016**, *120*, 349-56. DOI
53. Li, D.; Zhou, J.; Chen, X.; Song, H. Achieving ultrafast and stable Na-ion storage in $FeSe_2$ nanorods/graphene anodes by controlling the surface oxide. *ACS. Appl. Mater. Interfaces.* **2018**, *10*, 22841-50. DOI
54. Pan, Q.; Zhang, M.; Zhang, L.; et al. $FeSe_2$@C microrods as a superior long-life and high-rate anode for sodium ion batteries. *ACS. Nano.* **2020**, *14*, 17683-92. DOI
55. Zhou, S.; Jiang, R.; Wang, S.; et al. $FeSe_2$ micro-nanorods confined in N-doped carbon as an advanced anode for fast sodium ion storage. *J. Mater. Chem. A.* **2024**, *12*, 11028-37. DOI
56. Men, S.; Lin, J.; Zhou, Y.; Kang, X. N-doped porous carbon wrapped $FeSe_2$ nanoframework prepared by spray drying: a potential large-scale production technique for high-performance anode materials of sodium ion batteries. *J. Power. Sources.* **2021**, *485*, 229310. DOI
57. Yousaf, M.; Wang, Z.; Wang, Y.; et al. Core-shell $FeSe_2$/C nanostructures embedded in a carbon framework as a free standing anode for a sodium ion battery. *Small* **2020**, *16*, e2002200. DOI
58. Tian, W.; Ma, W.; Feng, Z.; et al. Formation of hierarchical Fe_7Se_8 nanorod bundles with enhanced sodium storage properties. *J. Energy. Chem.* **2020**, *44*, 97-105. DOI
59. Liu, T.; Li, Y.; Zhao, L.; et al. In situ fabrication of carbon-encapsulated Fe_7X_8 (X = S, Se) for enhanced sodium storage. *ACS. Appl. Mater. Interfaces.* **2019**, *11*, 19040-7. DOI
60. Chen, S.; Huang, S.; Zhang, Y. F.; et al. Constructing stress-release layer on Fe_7Se_8-based composite for highly stable sodium-storage. *Nano. Energy.* **2020**, *69*, 104389. DOI
61. Yuan, J.; Gan, Y.; Xu, X.; et al. Construction of Fe_7Se_8@Carbon nanotubes with enhanced sodium/potassium storage. *J. Colloid. Interface. Sci.* **2022**, *626*, 355-63. DOI
62. Yang, S.; Jiang, J.; He, W.; et al. Nitrogen-doped carbon encapsulating Fe_7Se_8 anode with core-shell structure enables high-performance sodium-ion capacitors. *J. Colloid. Interface. Sci.* **2023**, *630*, 144-54. DOI
63. Sun, Z.; Wu, X.; Gu, Z.; et al. Rationally designed nitrogen-doped yolk-shell Fe_7Se_8/Carbon nanoboxes with enhanced sodium storage in half/full cells. *Carbon* **2020**, *166*, 175-82. DOI
64. Wang, L.; Zhao, Y.; Chang, Y.; Zhu, S.; Qi, X. Carbon nanotube interweaved Fe_7Se_8 nanosheet/nanorod hybrids on expanded graphite for high-performance sodium storage. *J. Energy. Storage.* **2024**, *95*, 112593. DOI
65. Zhang, D. M.; Jia, J. H.; Yang, C. C.; Jiang, Q. Fe_7Se_8 nanoparticles anchored on N-doped carbon nanofibers as high-rate anode for sodium-ion batteries. *Energy. Storage. Mater.* **2020**, *24*, 439-49. DOI
66. Yang, Q.; Li, W.; Chou, S.; Wang, J.; Liu, H. Ball-milled FeP/graphite as a low-cost anode material for the sodium-ion battery. *RSC. Adv.* **2015**, *5*, 80536-41. DOI
67. Xu, X.; Feng, J.; Liu, J.; et al. Robust spindle-structured FeP@C for high-performance alkali-ion batteries anode. *Electrochim. Acta.* **2019**, *312*, 224-33. DOI
68. Li, Z.; Zhao, H.; Du, Z.; Zhao, L.; Wang, J.; Zhang, Z. Iron phosphide@N-doped carbon nanosheets with open-framework structure as an ultralong lifespan and outstanding rate performance electrode material for sodium-ion batteries. *J. Power. Sources.* **2020**, *465*, 228253. DOI
69. Wang, X.; Chen, K.; Wang, G.; Liu, X.; Wang, H. Rational design of three-dimensional graphene encapsulated with hollow FeP@carbon nanocomposite as outstanding anode material for lithium ion and sodium ion batteries. *ACS. Nano.* **2017**, *11*, 11602-16. DOI
70. Jiang, J.; Ma, C.; Zhang, W.; He, Y.; Li, X.; Yuan, X. Controlled design for integration of FeP into 3D carbon frameworks for superior Na storage. *Chem. Eng. J.* **2022**, *429*, 132271. DOI
71. Shi, S.; Li, Z.; Shen, L.; et al. Electrospun free-standing FeP@NPC film for flexible sodium ion batteries with remarkable cycling stability. *Energy. Storage. Mater.* **2020**, *29*, 78-83. DOI
72. Park, S.; Kim, C. W.; Lee, K. S.; Hwang, S. J.; Piao, Y. A densely packed air-stable free-standing film with FeP nanoparticles@C@P-doped reduced graphene oxide for sodium-ion batteries. *Nanoscale* **2023**, *15*, 14155-64. DOI
73. Wang, Y.; Zhou, P.; Zhang, M.; et al. High-performance honeycombed FeF_3@C cathodes enabling practical lithium pouch cells and silicon-metal fluoride batteries. *Energy. Storage. Mater.* **2023**, *60*, 102847. DOI

74. Zhang, L.; Ji, S.; Yu, L.; Xu, X.; Liu, J. Amorphous FeF_3/C nanocomposite cathode derived from metal-organic frameworks for sodium ion batteries. *RSC. Adv.* **2017**, *7*, 24004-10. DOI
75. Sun, Z.; Fu, W.; Liu, M. Z.; et al. A nanoconfined iron (iii) fluoride cathode in a NaDFOB electrolyte: towards high-performance sodium-ion batteries. *J. Mater. Chem. A.* **2020**, *8*, 4091-8. DOI
76. Sun, Z.; Wang, B.; Boebinger, M. G.; et al. Stability of FeF_3-based sodium-ion batteries in nonflammable ionic liquid electrolytes at room and elevated temperatures. *ACS. Appl. Mater. Interfaces.* **2022**, *29*, 33447-56. DOI
77. Ma, D.; Wang, H.; Li, Y.; et al. In situ generated FeF_3 in homogeneous iron matrix toward high-performance cathode material for sodium-ion batteries. *Nano. Energy.* **2014**, *10*, 295-304. DOI
78. Maulana, A. Y.; Song, J.; Futalan, C. M.; Kim, J. Improved reversibility of phase transformations using electron-rich graphitic carbon matrix in FeF_2 cathode for sodium-ion batteries. *Chem. Eng. J.* **2022**, *434*, 134727. DOI
79. Ni, D.; Fang, L.; Sun, W.; et al. FeF_2@MHCS cathodes with high capacity and fast sodium storage based on nanostructure construction. *ACS. Appl. Energy. Mater.* **2020**, *3*, 10340-8. DOI
80. Ni, D.; Sun, W.; Lu, C.; et al. Improved rate and cycling performance of FeF_2-rGO hybrid cathode with poly (acrylic acid) binder for sodium ion batteries. *J. Power. Sources.* **2019**, *413*, 449-58. DOI
81. Liu, M.; Wang, X.; Zhang, R.; et al. Hollow porous $FeF_3 \cdot 0.33H_2O$ microspheres by $AlPO_4$ coating as a cathode material of Na-ion batteries. *J. Energy. Storage.* **2018**, *18*, 103-11. DOI
82. Brugnetti, G.; Fiore, M.; Lorenzi, R.; Paleari, A.; Ferrara, C.; Ruffo, R. $FeTiO_3$ as anode material for sodium-ion batteries: from morphology control to decomposition. *ChemElectroChem* **2020**, *7*, 1713-22. DOI
83. Lin, Z.; Zhang, H.; Yang, C.; et al. Constructing $FeTe_2$ nanoparticles embedded in N-doped carbon nanofiber composites as a long-life and high-rate anode material for sodium-ion batteries. *Sustain. Energy. Fuels.* **2024**, *8*, 934-41. DOI
84. Ding, Y.; Chen, Y.; Xu, N.; et al. Facile synthesis of $FePS_3$ nanosheets@MXene composite as a high-performance anode material for sodium storage. *Nanomicro. Lett.* **2020**, *12*, 54. DOI PubMed PMC
85. Kim, J.; Kim, H.; Kang, K. Conversion-based cathode materials for rechargeable sodium batteries. *Adv. Energy. Mater.* **2018**, *8*, 1702646. DOI
86. Xu, S.; Dong, H.; Yang, D.; et al. Promising cathode materials for sodium-ion batteries from lab to application. *ACS. Cent. Sci.* **2023**, *9*, 2012-35. DOI PubMed PMC
87. Zheng, Y.; Zhang, Z.; Jiang, X.; et al. A comprehensive review on iron-based sulfate cathodes for sodium-ion batteries. *Nanomaterials* **2024**, *14*, 1915. DOI PubMed PMC
88. Zhang, Z.; Du, Y.; Wang, Q. C.; et al. A yolk-shell-structured $FePO_4$ cathode for high-rate and long-cycling sodium-ion batteries. *Angew. Chem. Int. Ed.* **2020**, *59*, 17504-10. DOI
89. Park, H.; Yoo, J. K.; Ko, W.; et al. Monoclinic $Fe_2(SO_4)_3$: a new Fe-based cathode material with superior electrochemical performances for Na-ion batteries. *J. Power. Sources.* **2019**, *434*, 226750. DOI
90. Hu, H.; Zhang, X.; Gao, Z.; et al. Boosting the cycle performance of iron trifluoride based solid state batteries at elevated temperatures by engineering the cathode solid electrolyte interface. *Small* **2024**, *20*, e2307116. DOI
91. Chu, Y.; Mu, Y.; Zou, L.; et al. Thermodynamically stable dual-modified LiF&FeF_3 layer empowering Ni-rich cathodes with superior cyclabilities. *Adv. Mater.* **2023**, *35*, e2212308. DOI
92. Hu, J.; Lei, M.; Zhu, C.; Zhang, B.; Li, C. Highly conductive doped fluoride solid electrolytes with solidified ionic liquid to enable reversible FeF_3 conversion solid state batteries. *Adv. Funct. Mater.* **2024**, *34*, 2314044. DOI
93. Wang, X.; Wang, Z.; Chen, L.; Li, H.; Wu, F. High-capacity sulfide all-solid-state lithium battery with a conversion-type iron fluoride cathode. *J. Mater. Chem. A.* **2023**, *11*, 4142-54. DOI